



CIVIL ENGINEERING STUDIES

Illinois Center for Transportation Series No. 22-014

UILU-ENG-2022-2014

ISSN: 0197-9191

Aerodynamic Survey of Novel eVTOL Configuration Using SU2

Prepared By

Wanzheng Zheng

Jason M. Merret

University of Illinois Urbana-Champaign

Research Report No. I-ACT-21-04

A report of the findings of

I-ACT PROJECT 21-04
eVTOL Configuration Understanding,
Development, and Design

<https://doi.org/10.36501/0197-9191/22-014>

Illinois Center for Transportation

August 2022

TECHNICAL REPORT DOCUMENTATION PAGE

1. Report No. I-ACT-21-04	2. Government Accession No. N/A	3. Recipient's Catalog No. N/A	
4. Title and Subtitle Aerodynamic Survey of Novel eVTOL Configuration Using SU2		5. Report Date August 2022	
		6. Performing Organization Code N/A	
7. Authors Wanzheng Zheng and Jason M. Merret	8. Performing Organization Report No. ICT-22-014 UILU-ENG-2022-2014		
9. Performing Organization Name and Address Illinois Center for Transportation Department of Civil and Environmental Engineering University of Illinois at Urbana-Champaign 205 North Mathews Avenue, MC-250 Urbana, IL 61801		10. Work Unit No. N/A	
		11. Contract or Grant No. I-ACT-21-04	
12. Sponsoring Agency Name and Address		13. Type of Report and Period Covered Final Report 3/16/21–8/30/22	
		14. Sponsoring Agency Code	
15. Supplementary Notes Conducted in cooperation with the Illinois Center for Transportation. https://doi.org/10.36501/0197-9191/22-014			
16. Abstract This report summarizes computational fluid dynamics (CFD) results of electric vertical takeoff and landing (eVTOL) geometries using the SU2 Reynolds-averaged Navier-Stokes (RANS) solver. Geometries were generated based on the Smart Transportation Infrastructure Initiative (STII) Rappor 15th iteration with various rotor-installment solutions. It was found that although open rotors installed on an underwing pylon were superior to shrouded rotors installed in a canoe, the canoe configuration would provide more potential for improvement, and using a canoe door to cover the first rotor opening would reduce the drag experienced by the canoe case below that upon the rod case. Rotor doors were found to be most efficient in reducing drag of the canoe case: Average drag reduction with covering the first rotor and all rotors was 66 and 165 counts, respectively. Changing rotor distributions along the chordwise direction had minimal impact on drag reduction, and placing rotors along the spanwise direction was not advised due to the increase of the projected frontal area. Increasing canoe chord length did not have significant impact on drag reduction; and if rotor doors were implemented, increasing canoe size had negative impact on drag. Rounding rotor edges did not change the aerodynamic performance of the canoe case but promotes vertical air intake when running lifting fans. Drag received by the canoe parabolically correlated to rotor diameter, with 126 counts of drag if the rotor diameter was 0 and 377 counts if the rotor diameter was 2.95 ft. Fuselage and tail added an average 179 counts of drag, and thus the aforementioned differences were still significant in the scale of aerodynamic properties of the full configuration.			
17. Key Words Aerodynamics, Air-Taxi Service, eVTOL CFD, Open Rotors, Shrouded Rotors, Urban Air Mobility, SU2		18. Distribution Statement No restrictions. This document is available through the National Technical Information Service, Springfield, VA 22161.	
19. Security Classif. (of this report) Unclassified	20. Security Classif. (of this page) Unclassified	21. No. of Pages 35	22. Price N/A

ACKNOWLEDGMENT, DISCLAIMER, MANUFACTURERS' NAMES

This publication is based on the results of **I-ACT-21-04: eVTOL Configuration Understanding, Development, and Design**. I-ACT-21-04 was conducted in cooperation with the Illinois Center for Transportation.

The contents of this report reflect the view of the authors, who are responsible for the facts and the accuracy of the data presented herein. The contents do not necessarily reflect the official views or policies of the Illinois Center for Transportation. This report does not constitute a standard, specification, or regulation.

Trademark or manufacturers' names appear in this report only because they are considered essential to the object of this document and do not constitute an endorsement of product by the Illinois Center for Transportation.

EXECUTIVE SUMMARY

The concept of a vertical takeoff vehicle—or informally, a flying car—is an idea with a long history in the field of aviation. Recent advances in electrochemical power have generated a significant resurgence of interest in electric vertical takeoff-and-landing vehicle (eVTOL) aircraft [1]. An eVTOL is defined as a vertical-lift aircraft propelled by electric power and capable of carrying people. Since the emergence of the National Aeronautics and Space Administration (NASA) Puffin eVTOL concept in 2009 [2], several industrial efforts were made, following which the concept was officially introduced by the Vertical Flight Society and the American Institute of Aeronautics and Astronautics in 2014 [3].

Foreseeable eVTOL civil applications ranged from delivery of passengers or packages to provision of emergency responses in a versatile manner. The novel vehicle concept could fulfill the role of conventional helicopters, while offering the promise of safer, cleaner, quieter, and potentially cheaper operations. Companies, ranging from established aerospace corporations like Boeing and Airbus to start-up companies like Lilium and Joby, were currently working on their own versions of eVTOL, providing the market with various unique concepts of eVTOL design [4].

With the choices available for the initial sizing of new vehicle designs, it was natural to question which type of configuration would be most suitable. To provide a quantitative answer from an aerodynamic perspective to the problem posted above, two configurations were developed from Smart Transportation Infrastructure Initiative (STII) geometry, one with open rotors installed on a rod under the wing and one with shrouded rotors installed in the wing; these configurations were simulated and compared. Simulations were also performed to investigate the sensitivity of aerodynamic coefficients to other potential design variables.

It was observed that, if no additional elements were added, the rod with open-rotor configuration was slightly superior to the canoe with shrouded rotors. However, if rotor doors were taken into consideration, the canoe case had great potential for improvement, experiencing up to 26% less drag than the rod case. Covering the leading-edge rotors provided the most drag reduction, and covering just the first rotor would provide a canoe configuration with better aerodynamic properties than the rod case. Lift and drag of the canoe case were relatively insensitive to design variables such as leading-edge thickness, rotor distribution, and canoe chord length, providing freedom of modification with little change in aerodynamic properties.

Findings of this report suggested that a configuration with a canoe and shrouded rotor installed within should be used if the vehicle were intended to cruise with a fixed wing for better aerodynamic performance. This report also suggested that rotor openings should be covered as much as possible, starting from the leading-edge rotors.

TABLE OF CONTENTS

CHAPTER 1: INTRODUCTION	1
CHAPTER 2: METHODS AND VERIFICATIONS.....	3
GEOMETRY AND CFD METHODS	3
CONVERGENCE AND VALIDATION STUDY.....	6
CHAPTER 3: ROD AND CANOE CONFIGURATIONS	9
CHAPTER 4: VARIATION IN SENSITIVITY OF CANOE CASE	12
EFFECT OF CANOE THICKNESS.....	12
EFFECT OF CANOE DOORS	12
EFFECT OF ROTOR PLACEMENT.....	18
EFFECT OF LEADING-EDGE MODIFICATIONS.....	22
EFFECT OF ROUNDING ROTOR EDGES	26
EFFECT OF ROTOR DIAMETERS	27
CHAPTER 5: FULL-CONFIGURATION SURVEY.....	30
CHAPTER 6: CONCLUSION AND FUTURE WORK	32
REFERENCES.....	35

LIST OF FIGURES

Figure 1. Photos of eVTOL designs of various categories.....	1
Figure 2. CAD model of the rod case.	4
Figure 3. CAD model of the canoe case.....	5
Figure 4. Y+ value of baseline cases.	6
Figure 5. Surface mesh of convergence study.....	7
Figure 6. Convergence of drag coefficient for the test case.	7
Figure 7. Geometry simulated for validation study with rotor openings numbering.....	8
Figure 8. Comparison among predictions of various CFD methods.	8
Figure 9. Aerodynamic differences with rotor addition.....	9
Figure 10. CAD model of canoe and rod (single and double column) configurations with wing.....	10
Figure 11. Aerodynamic properties of canoe and rod (single and double column) configurations with wing.....	11
Figure 12. CAD of canoe case with various canoe thicknesses.	13
Figure 13. Aerodynamic properties of canoe case with various canoe thicknesses.....	13
Figure 14. CAD model of canoe case, with rotor naming.....	14
Figure 15. Aerodynamic properties of canoe case with covering of first and second rotor openings..	14
Figure 16. Aerodynamic properties of canoe case with covering of individual rotor openings.	15
Figure 17. Aerodynamic properties of canoe case with covering of consecutive rotor openings.....	16
Figure 18. CAD model of canoe case integrated with wing.	17
Figure 19. Aerodynamic properties of canoe cases integrated with wing.....	17
Figure 20. CAD of canoe case with various rotor-placement methods.	19
Figure 21. Aerodynamic properties of canoe case with various rotor placements.	19
Figure 22. Visualization of CF distribution of canoe case with various rotor placements.....	20
Figure 23. CAD of canoe case with various rotor chordwise distributions.	20
Figure 24. Aerodynamic properties of canoe case with various rotor chordwise distributions.....	21
Figure 25. Pressure comparison of canoe sections with various rotor chordwise distributions.	21
Figure 26. CAD of canoe case with various canoe chord lengths.....	23
Figure 27. Aerodynamic properties of canoe case with various canoe chord lengths.	23

Figure 28. L/D of canoe case with various canoe chord length at an 8-degree angle of attack.....	24
Figure 29. CAD of canoe case with various canoe chord lengths, with rotor 1 covered.	24
Figure 30. Aerodynamic properties of canoe case with various chord lengths, rotor 1 covered.....	25
Figure 31. Cp distribution of canoe case with rounded rotor edge.	26
Figure 32. Pressure comparison of canoe section with rounded rotor edge.....	26
Figure 33. Aerodynamic properties of canoe case with rounded rotor edge.....	27
Figure 34. CAD of canoe case with various rotor diameters.....	28
Figure 35. Aerodynamic properties of canoe case with various rotor diameters.....	28
Figure 36. L/D contour of canoe case with various rotor diameters.	29
Figure 37. CAD of canoe and rod cases with fuselage and tail.....	30
Figure 38. Aerodynamic properties of full configurations.	31
Figure 39. Cp distribution of full configurations.....	31
Figure 40. CAD of possible new configuration.	34

LIST OF TABLES

Table 1. Simulation Environments.....	3
Table 2. Drag Reduction with Covering of Consecutive Rotor Openings	15
Table 3. Average Drag Difference for Various Rotor Chordwise Distributions	20
Table 4. Average Drag Difference for Various Canoe Chord Lengths.....	25
Table 5. Summary of Trade Elements and Respective Drag Differences	33

CHAPTER 1: INTRODUCTION

Electric vertical takeoff-and-landing (eVTOL) aircraft have generated significant interest, thanks to their versatile applications and recent advances in electrochemical power [1, 3]. The novel vehicle concept could fulfill the role of conventional helicopters, while offering the promise of safer, cleaner, quieter, and potentially cheaper operation. Companies—ranging from established aerospace corporations like Boeing and Airbus to start-ups like Lilium and Joby—are currently working on their own versions of eVTOL, providing the market with various unique concepts of eVTOL design [4]. Generally, classification of eVTOL could be made on their operation mechanism and configuration. A few current configurations that are representative of their respective design philosophies are presented in Figure 1 [5–9]. Designs that depend on rotors to provide lift and thrust include electric helicopter and multi-copter, and designs that require wings to provide lift during cruise include tilt-rotor design, fixed-wing with vector-thrust design, and lift-and-cruise hybrid design [10]. An initial sizing study suggested that all-rotor configurations required higher energy demands and thus were feasible only for shorter ranges [11]. For this project, the lift-and-cruise hybrid design was chosen as baseline due to the high range requirement for an air taxi.

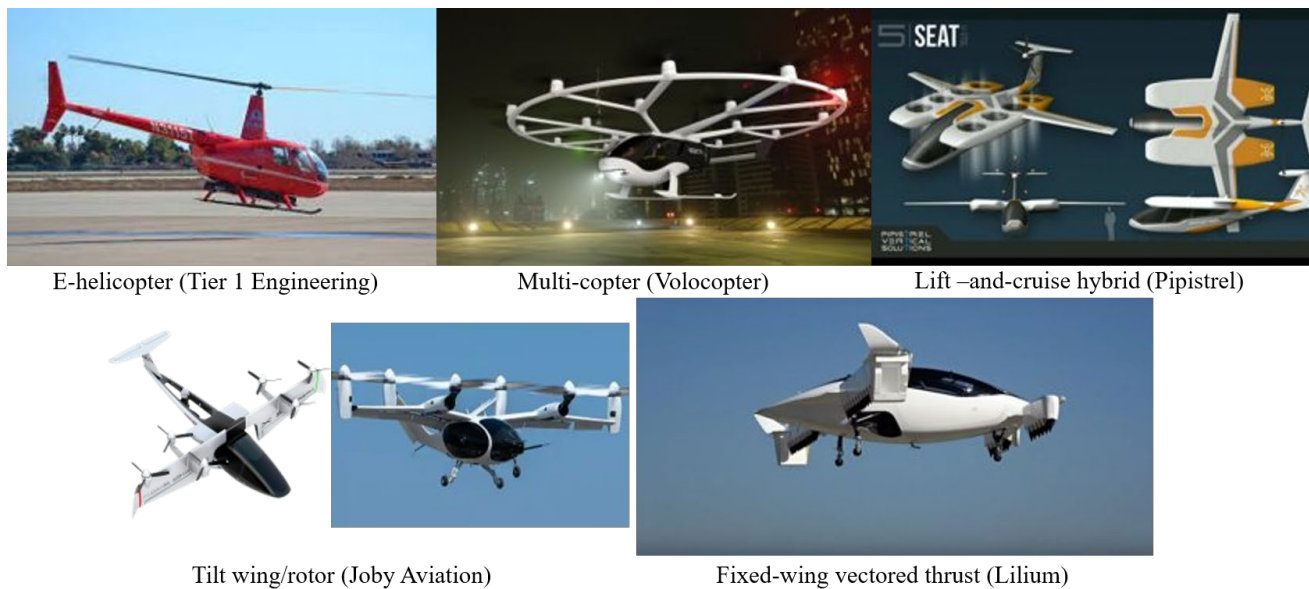


Figure 1. Photos of eVTOL designs of various categories.

Sources: [5–9]

Current winged eVTOL configurations seen on the market often feature open rotors installed on underwing pylons (rods) to achieve vertical takeoff and landing. Although such configurations were the most intuitive and perhaps easiest to accomplish from an integrated standpoint, with the development of the eVTOL industry, novel designs using shrouded rotors are also becoming popular. With the choices available for the initial sizing of new vehicle designs, it was natural to question which type of configuration was most suitable for the intended mission profile. To provide a quantitative answer from an aerodynamic perspective to the problem posted above, two

configurations were developed from STII geometry, one with open rotors installed on a rod under the wing and one with shrouded rotors installed in the wing (canoe); these configurations were simulated and compared. Simulations were also performed to ascertain the sensitivity of other potential design variables, namely rotor sizing and spacing, canoe thickness, and rotor doors.

This report provides simulation results of the aforementioned configurations, as well as other variations derived from the baseline geometry using SU2 computational fluid dynamics (CFD) packages. Basic explanations of geometries and simulation methods are given in Chapter 2.

Comparison between different means of installing rotors is made in Chapter 3. Derivative geometries by varying design parameters are investigated in Chapter 4 to determine the driving factors of aerodynamic performance of the shrouded-rotor configuration. A batch of simulations on various wing designs on fuselage are made in Chapter 5 to determine the significance of the discussions in previous chapters. Finally, in Chapter 6, conclusions are drawn from presented data to offer qualitative to semi-quantitative suggestions for future iterations of this eVTOL vehicle.

CHAPTER 2: METHODS AND VERIFICATIONS

GEOMETRY AND CFD METHODS

The current configuration of interest was built upon the 15th iteration of the STII Rappor design. The first 14 iterations varied in wing and other basic factors of vehicle sizing and resulted in a semidefinite design that forms the basis of this study. A schematic of the full-scale geometry is presented in Figure 2 and Figure 3, in which the main interest of this study focused on the wing and rotor placements.

The canoe consists of an National Advisory Committee for Aeronautics (NACA) 0006 airfoil with a span of 20 ft and a width of 4 ft. The rod has a diameter of 1 ft and was rounded at the two ends with hemispheres, and each hub has a diameter of 10 in. and a height of 11 in. Rotors are placed symmetrically with respect to the center chord, and the rotor size was chosen to be 1.96 ft and held constant unless it was a variable of interest. Two major configurations of interest were the shrouded rotor installed on a canoe, from here on referred to as the *canoe case*; and the open rotors installed under the wing, from here on referred to as the *rod case*. Because the rod case does not require an extended wing section to install shrouded rotors, the canoe was removed in the rod case with the root airfoil, and the wing airfoil was held at constant shape and position.

Aerodynamic performances were collected using the SU2 CFD Reynolds-averaged Navier-Stokes (RANS) solver [12] with flight condition set for 0.1 Mach at sea-level standard atmosphere, at angles of attack ranging from 0 to 8 degrees with 2-degree intervals. Variables of interest for this CFD simulation are listed in Table 1. The meshing of geometries was performed in Pointwise [13] using hybrid cells. The average cell size was chosen to be 0.01 to balance computational expenses and simulation accuracy. Details of the convergence study are presented in the following subchapter. Cell height on the wall cell height was later estimated to be 1.2E-5 with a normal growth rate of 1.2 to achieve a $y+$ value less or equal to 1. A surface $y+$ contour is presented in Figure 4. Surface $y+$ values were examined only for the baseline cases presented in Figure 2 and Figure 3, as the RANS solver could resolve high boundary-layer cells using wall functions. A semispherical domain was created and labeled as pressure far-field with respective Mach number and total pressure of the standard sea-level atmosphere. Convergence criterion was set so that the root mean square error of the drag coefficient was to be less than 1E-6. Results given in this report have all satisfied such convergence criterion.

Table 1. Simulation Environments

Variables	Metric Units	Imperial Units
Reynolds Number	12.3E+06	12.3E+06
Mach Number	0.1	0.1
Velocity	34.030 [m/s]	111.6 [ft/s]
Temperature	288.15 [K]	518.7 [R]
Characteristic Length	6 [m]	19.7 [ft]
Reference Area	15.236 [m ²]	163.9 [sq ft]

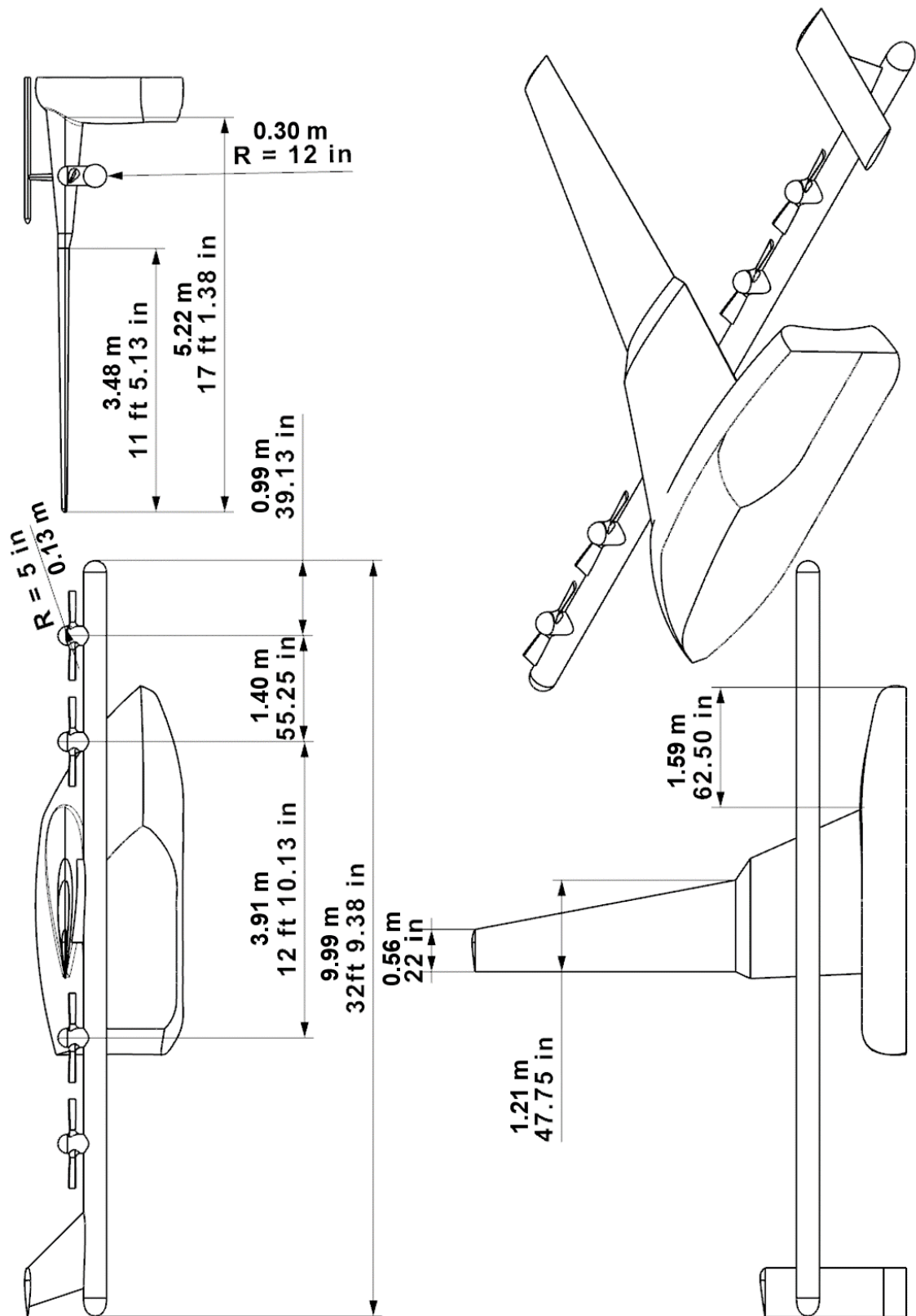


Figure 2. CAD model of the rod case.

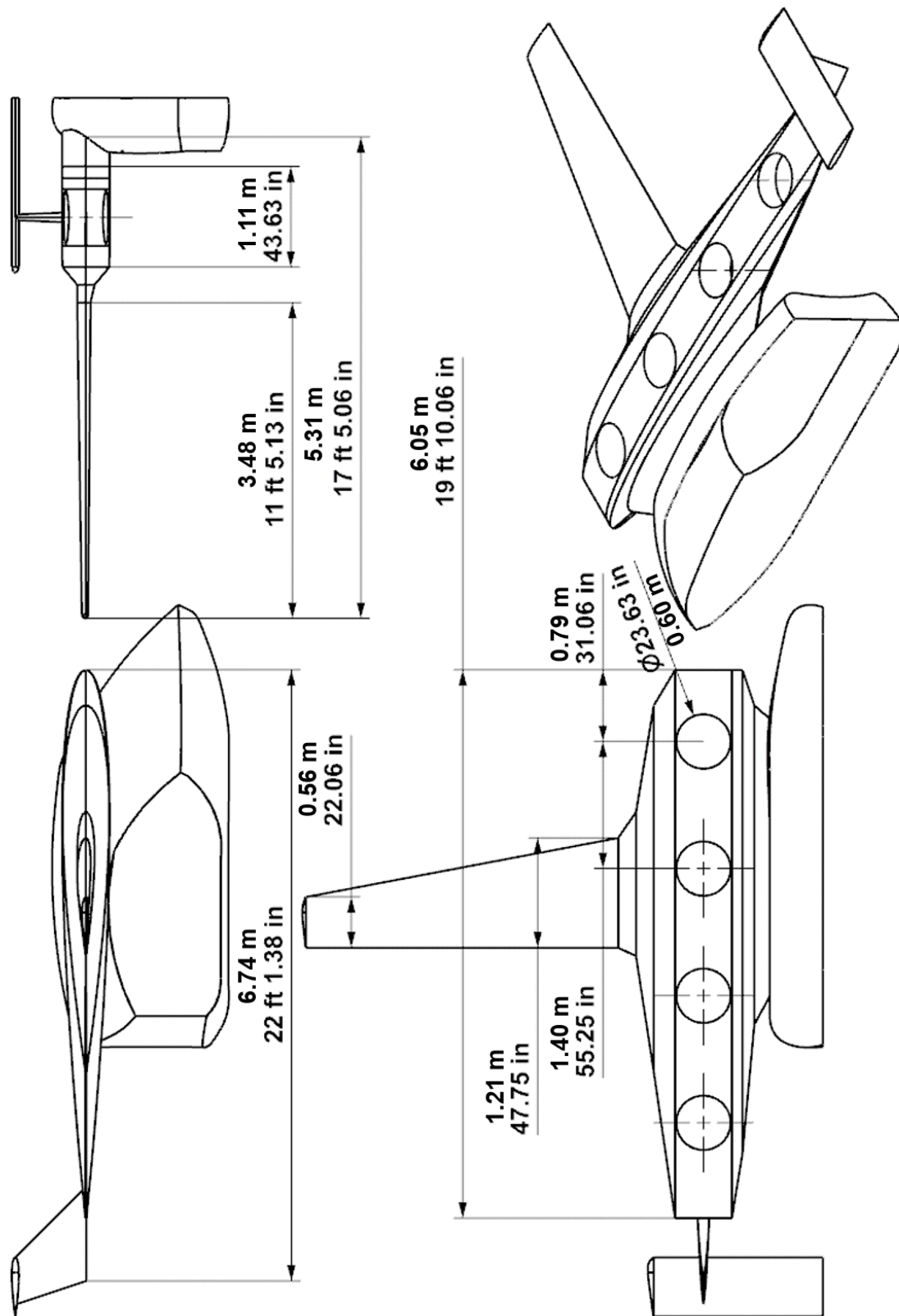


Figure 3. CAD model of the canoe case.

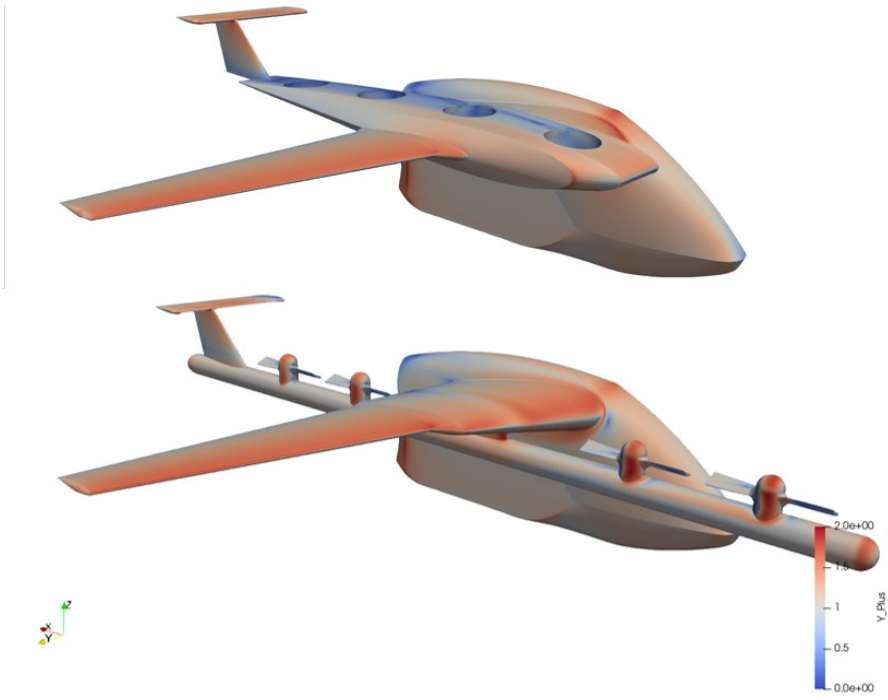


Figure 4. $Y+$ value of baseline cases.

CONVERGENCE AND VALIDATION STUDY

This study was intended to ensure the quality of the results. The problem was divided into three aspects, and each was investigated separately. It was well-known that the solver chosen for this study was dependent on cell quality and resolution of the mesh. A set of simulations was conducted to ensure adequate grid quality was applied, by running a convergence study on meshes with the same geometry and simulation conditions but different cell densities. Cell density was measured by average edge length between nodes on the surface mesh (Δs). Δs chosen for the convergence study ranged from overly coarse (0.02) to very fine (0.004); and convergence of the aerodynamic parameter should be observed in between, indicating an adequate mesh density that offers reliable results while remaining computationally efficient. A further validation study was conducted to ensure consistency of results by comparing simulation results from two different CFD methods. Finally, a comparison was made between the RANS solver and Euler's solver corrected by empirical methods to ensure the chosen turbulence model was correct.

The convergence study test case consisted of the wing part of the configurations of interest, presented in Figure 5. The mesh consists of fully structured mesh on the wing and unstructured mesh at the wing cap at tip of the wing. A further analysis was performed on the canoe case to ensure that convergence behavior was identical to that of the test case. The results of the convergence study are presented in Figure 6. A set of simulations that were more geometrically complex, as compared to the test case, was then conducted on just the canoe. The convergence trend of this simulation matched that observed in the convergence study. It was thus determined that an average cell size of 0.01 would suffice for the scope of this study, as its value deviates less than 3% from the converged value.

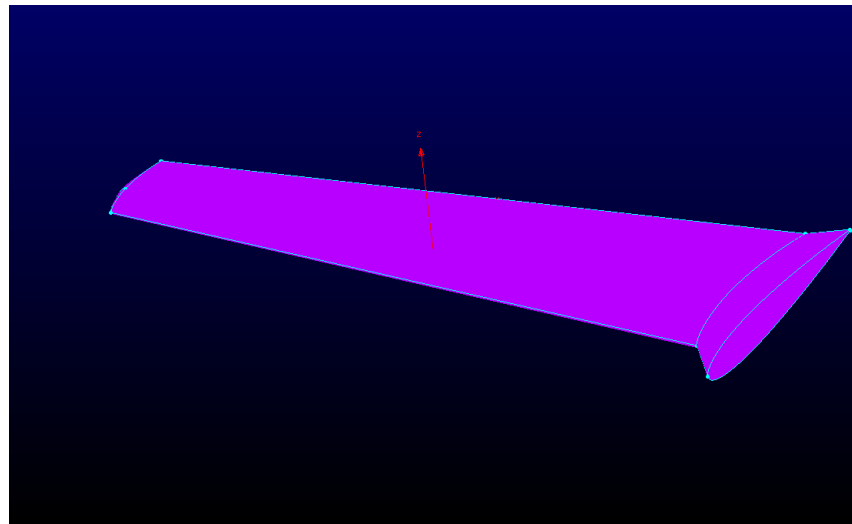


Figure 5. Surface mesh of convergence study.

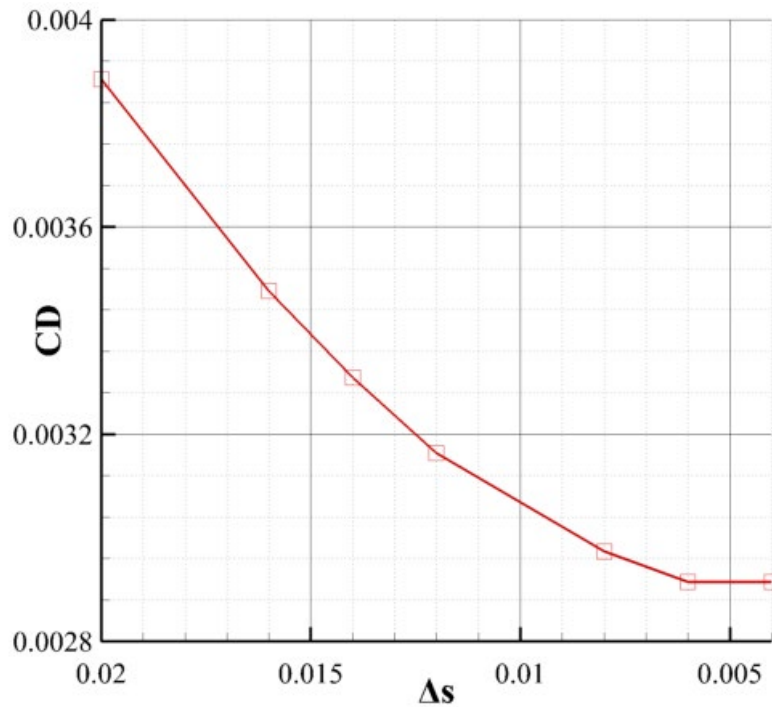


Figure 6. Convergence of drag coefficient for the test case.

A simulation was conducted, and results were compared with those predicted by a different CFD package: STAR CCM+. The configuration of interest consists of the canoe with no wing attached and various rotor openings covered, as presented in Figure 7. The verification used RANS solver from SU2 comparing the constant density equation of state with the SST K- ω turbulence model from STAR-CCM+. All initial conditions were set to those presented in Table 1. A comparison of the results is presented in Figure 8. The RANS solver in SU2 tends to overpredict drag, as compared to that

predicted by STAR CCM+; but overall, the comparison showed significant similarity between the results obtained from the two methods. Most importantly, the relative difference and the trend of aerodynamic coefficient to angles of attack were identical. This comparison and the display of encouraging similarity offered more confidence in the physical correctness of the SU2 predictions used later in this report. Another comparison was made for the rod case between the RANS solver and the Euler solver corrected by empirical methods. The two solvers of interest provided identical results in drag prediction, implying that the turbulence model of choice is accurate for the scope of this study. It should be noted that separated flow was not represented correctly with the choice of solver and turbulence model. However, the results presented were still valid for the purpose of comparison, which was the major interest of this study.

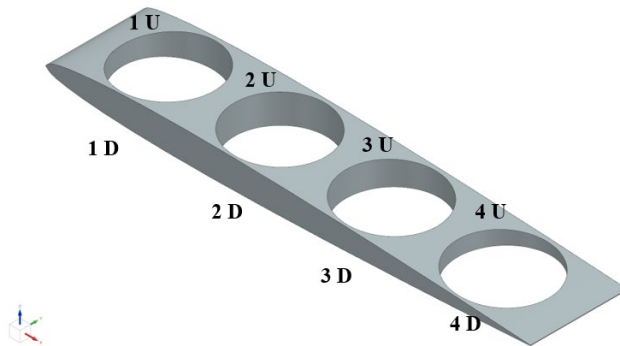


Figure 7. Geometry simulated for validation study with rotor openings numbering.

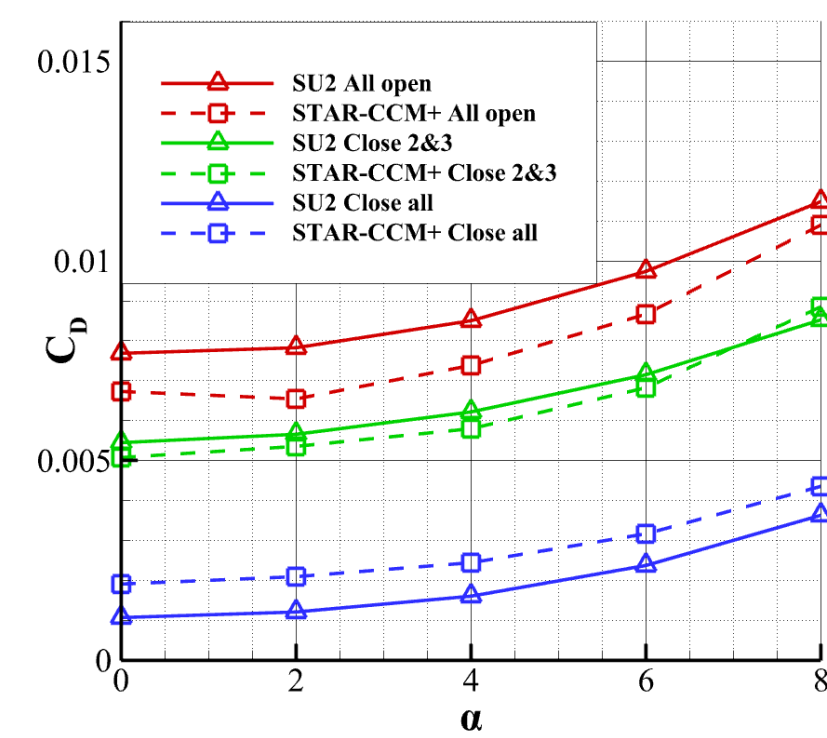


Figure 8. Comparison among predictions of various CFD methods.

CHAPTER 3: ROD AND CANOE CONFIGURATIONS

This report first discussed the effect on aerodynamic properties of including rotor blades. Simulations were performed on individual configurations with and without rotor blades installed. The results are presented in Figure 9. The three polars, from top left to bottom, were drag polar, lift coefficients versus angles of attack, and lift over drag (L/D) versus angles of attack. It was observed that adding rotors improves aerodynamic properties for the canoe case, while slightly worsening those for the rod case. Maximum differences on drag coefficient were around 20 counts, as compared to respective configurations without rotors. Adding rotors partially prevented recirculation in open shrouds for the canoe case, while provoking larger flow separation on the rod case, which explains why adding the same component may negatively impact drag characteristics for one configuration and positively impact the other. For the sake of simplicity, the effect of rotors was not considered for further simulations consisting of comparative features of the canoe. Note the decrease of L/D of the rod case at a 2-degree angle of attack was also observed in simulations conducted using STAR-CCM+. The reason for such phenomenon has not yet been investigated, as it was not among the major interests of this study.

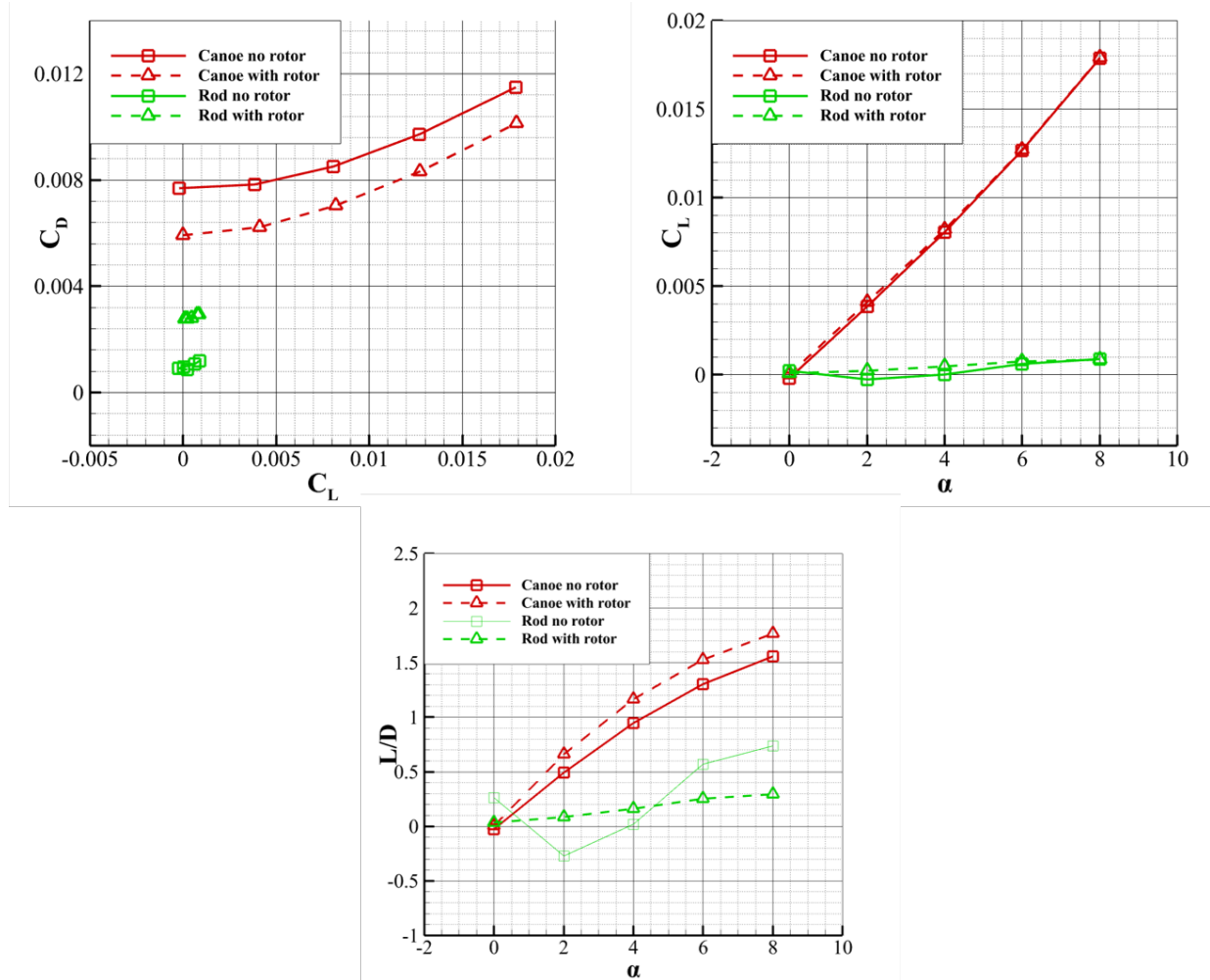


Figure 9. Aerodynamic differences with rotor addition.

The rod and canoe configurations were then integrated with the wing design of the 15th iteration, presented in Figure 10. A new configuration was added in which the rod was split in two and installed separately under the wing. Aerodynamic properties of the three configurations were compared in Figure 11.

The four polars, from top left to bottom right in Figure 11, were drag polar, lift coefficients versus angles of attack, lift over drag versus angles of attack, and induced drag over lift versus lift coefficients. The first plot quantitatively illustrates drag characteristics for various flight conditions, the second illustrates the sensitivity of lift with respect to vehicle orientation, and the last two illustrate lift over drag, which is related to the vehicles' range and endurance capability, and the efficiency factor that relates drag to lift squared. Four such plots are presented for further simulations to offer in-depth visualization of results and their implications.

It was observed that the canoe case has aerodynamic characteristics similar to those of the rod case at low angles of attack, but they quickly diverge as angles of attack increase and larger flow separation begins to occur. However, the canoe case has more possibilities for integrating elements such as canoe doors, which potentially would improve its aerodynamic performance. Further studies were conducted to quantitatively specify such potentials in the following sections. From an aerodynamic perspective, it is not advisable to use multiple underwing pylons because the increase in the frontal area increases drag.

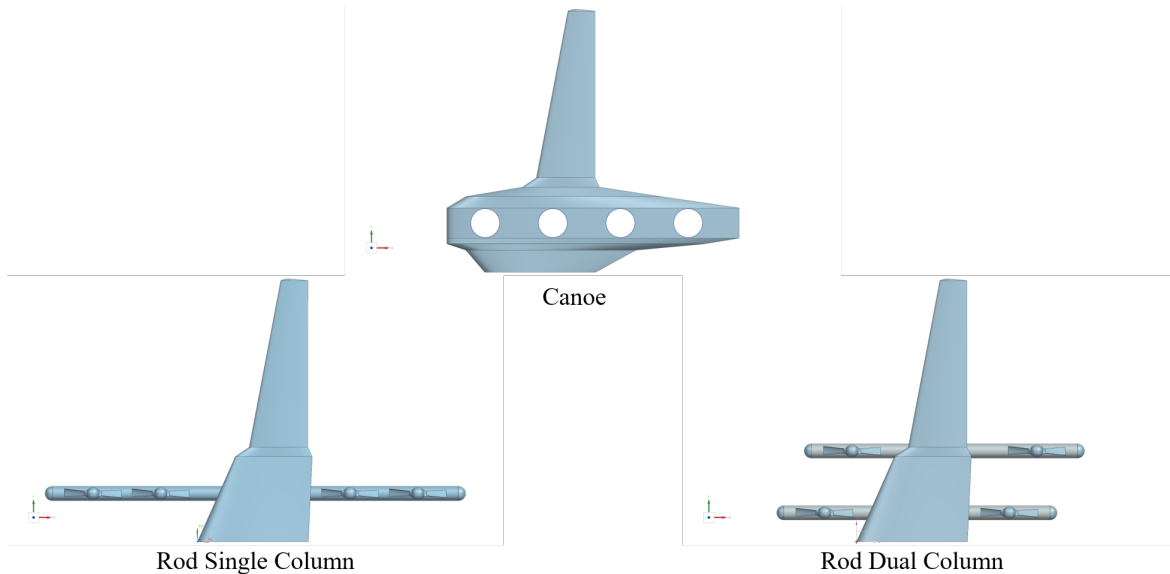


Figure 10. CAD model of canoe and rod (single and double column) configurations with wing.

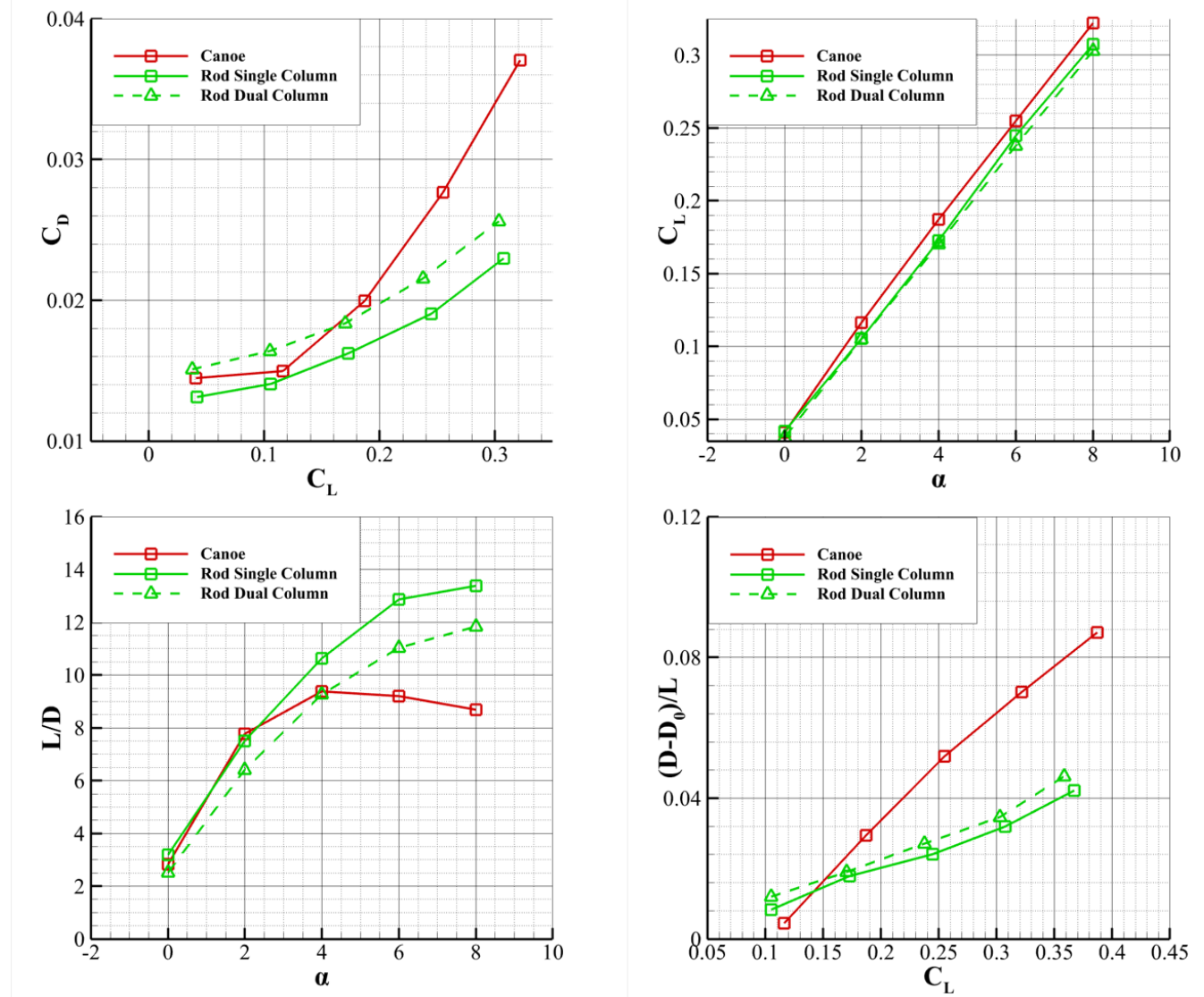


Figure 11. Aerodynamic properties of canoe and rod (single and double column) configurations with wing.

CHAPTER 4: VARIATION IN SENSITIVITY OF CANOE CASE

Implementing drag reduction modifications to wing designs would inevitably introduce more weight to the current design and cause new aeroelastic concerns, which change the nature of the problem of interest into a multi-objective, multidisciplinary optimization (MDO). Although the above optimization problem was not performed in this report, it would certainly be a function of the sensitivity of aerodynamic properties with respect to each potential design variable, either single or coupled. Therefore, this section aims to provide quantitative information on how each possible modification to the baseline case impacts the overall aerodynamic performance of the canoe case. In the future, the aforementioned MDO problem could be formulated and performed with additional considerations such as weight and the structural and intended mission profile of the vehicle.

EFFECT OF CANOE THICKNESS

As the stagnation in rotor openings has been acknowledged as a major source of drag, an investigation of varying canoe thickness was carried out. A thinner canoe would potentially decrease the frontal area of the vehicle. Two configurations of interest were modified, based on the canoe configuration; all rotors covered or all rotors open, with canoe thickness decreased by 25%. The models of interest are presented in Figure 12 and the simulation results in Figure 13. Varying canoe thickness does not significantly interfere with drag characteristics, as the modification resulted in, on average, fewer than 10 counts of drag difference from their baseline cases, respectively. Such minimal difference is likely due to the thickness of the canoe's already being thin, as compared to the chord length, as NACA 0006 was chosen to be the canoe airfoil.

EFFECT OF CANOE DOORS

Canoe doors could be added to prevent early separation caused by the installed shrouded rotors. A set of simulations was conducted to investigate whether covering the upper, the lower, or both of the shrouded rotors was necessary. A schematic of the canoe configuration with naming conventions is presented in Figure 14. Each rotor hole was covered individually on the suction, pressure, or both sides, namely X_U, X_D, and X_U/D, where X is the rotor number. The resulting polars of these cases are presented in Figure 15. Adding a canoe door improved the aerodynamic properties of the configuration; and covering the pressure, or lower, surface was slightly more efficient than covering the suction, or upper, surface. However, such differences were trivial compared to the drag reduction by covering both holes of the rotor; and thus, the option of closing only one surface of a rotor was not taken into further consideration. For simplicity in nomenclature, closing both upper and lower surfaces of any rotor openings was represented by the number of the respective openings alone, and the previously used subscripts of U/D were dropped.

It was also observed that covering the first rotor along the leading edge offered more drag reduction than covering the second rotor, as the pressure side experienced larger pressure differences. A survey was conducted to further solidify this speculation by covering each rotor hole, as presented in Figure 16. Drag reduction decreases as the rotor covered shifts from the leading edge to the trailing edge, and the maximum difference between these configurations of interest, namely cover 4 and

cover 1, was 16 counts on average. Thus, it was concluded that consecutive rotor openings, starting from the leading edge, should be covered to yield optimal drag reduction.

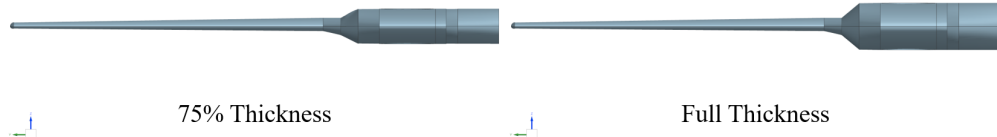


Figure 12. CAD of canoe case with various canoe thicknesses.

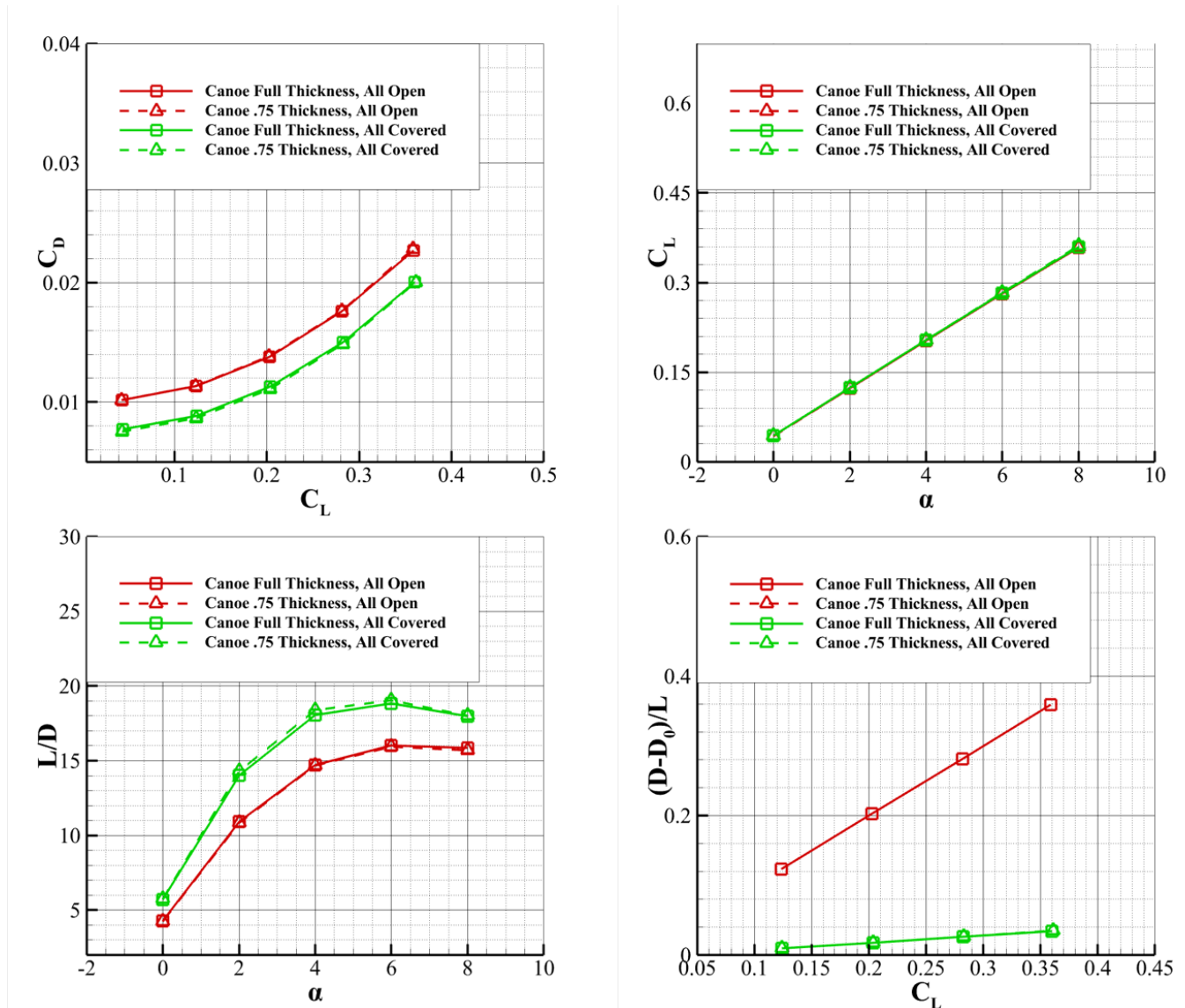


Figure 13. Aerodynamic properties of canoe case with various canoe thicknesses.

A wholistic survey was conducted to investigate the effect of covering openings of rotors in various positions. From previous results, only modifications of consecutive openings on both suction and pressure sides were considered. The polar of this survey is presented in Figure 17. Average reduction in drag with respect to the all-open case is presented in Table 2.

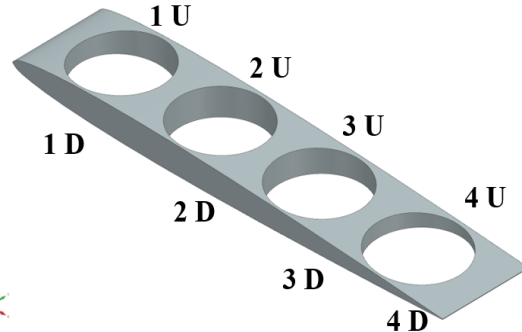


Figure 14. CAD model of canoe case, with rotor naming.

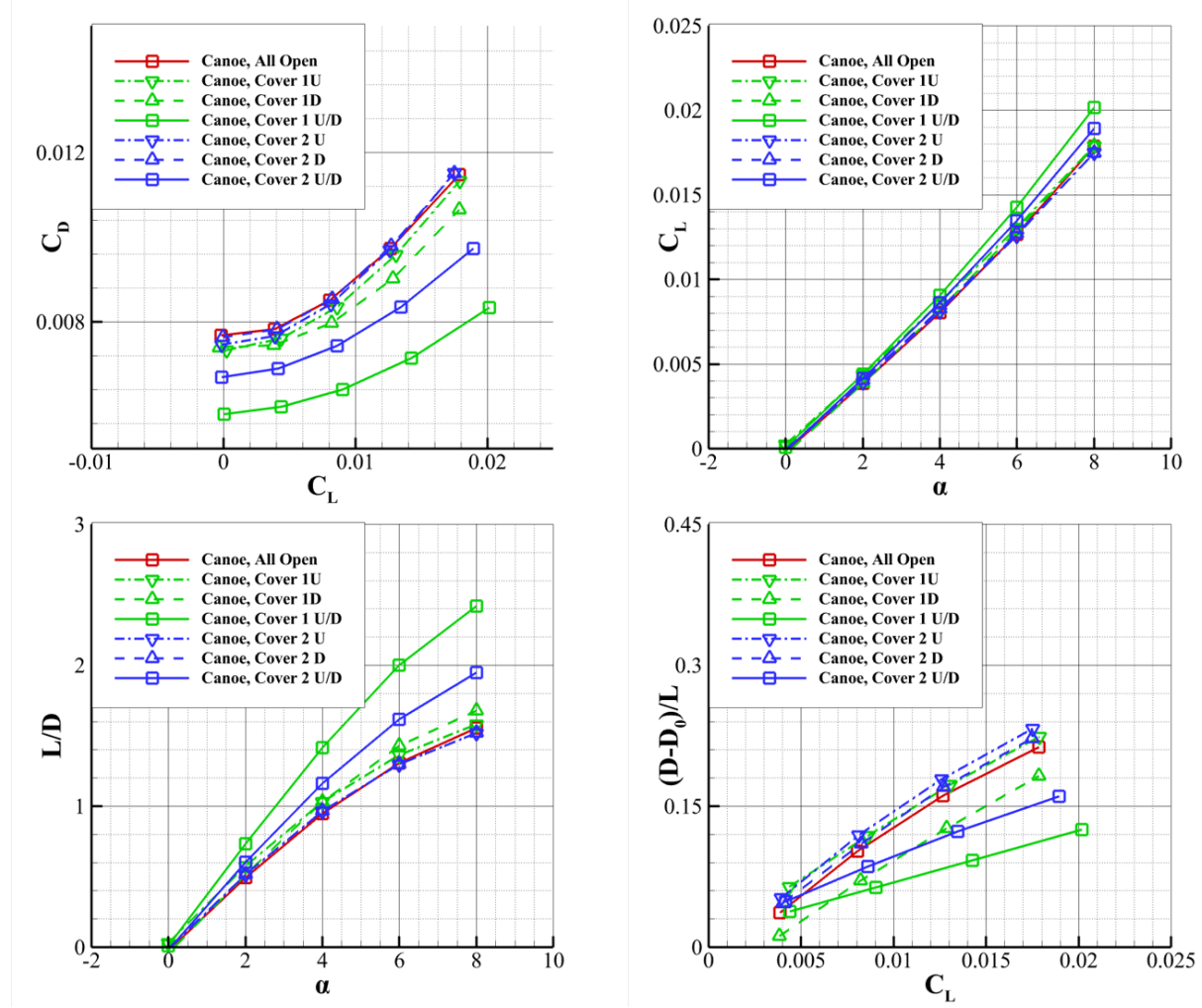


Figure 15. Aerodynamic properties of canoe case with covering of first and second rotor openings.

Table 2. Drag Reduction with Covering of Consecutive Rotor Openings

Configuration	Average Drag Reduction (counts)	Average Percent of Reduction
Close 1	23.1	25.5%
Close 1 and 2	36.3	40.1%
Close 1, 2, and 3	52.0	57.5%
Close 1, 2, 3, and 4	70.6	78.1%

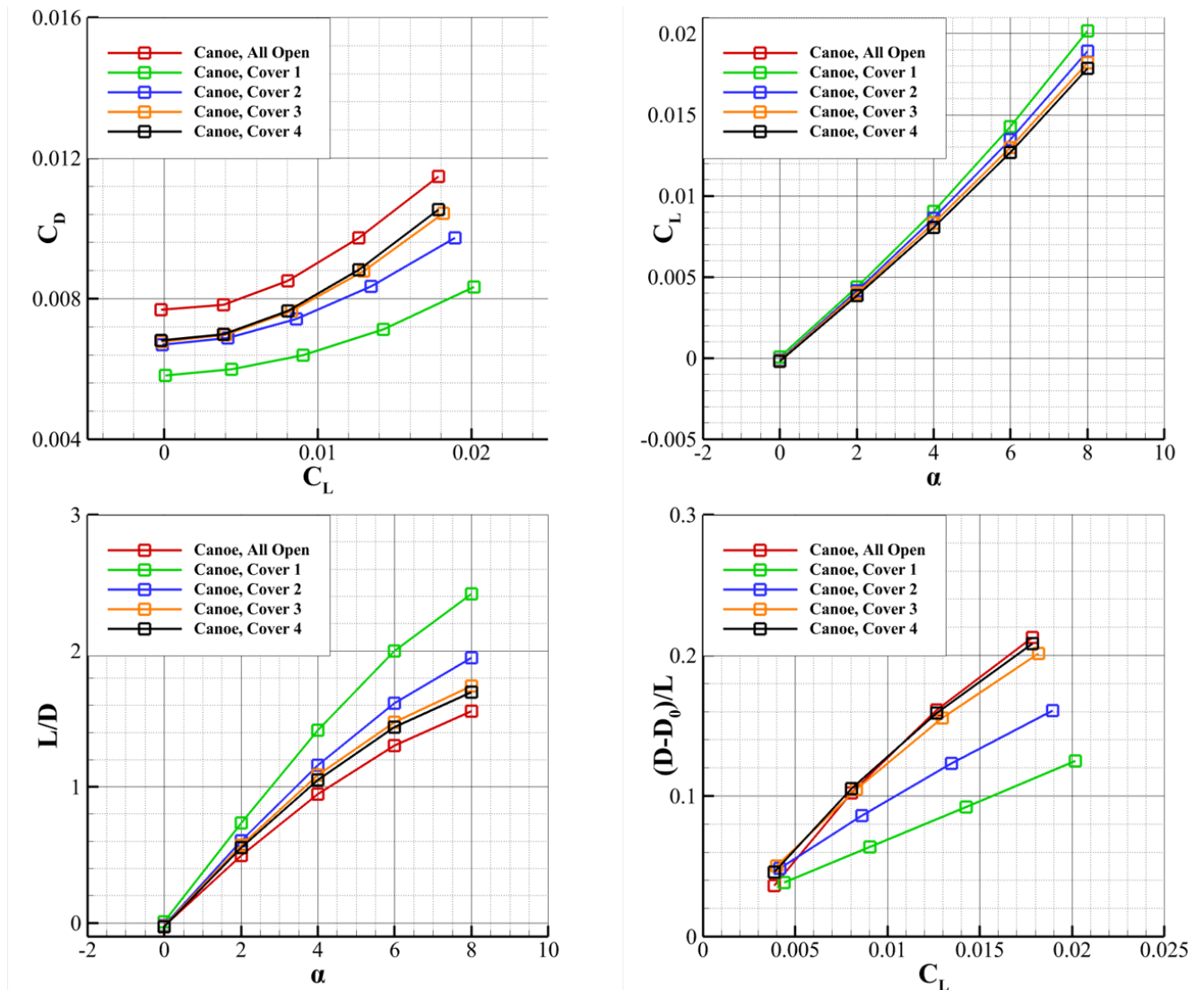


Figure 16. Aerodynamic properties of canoe case with covering of individual rotor openings.

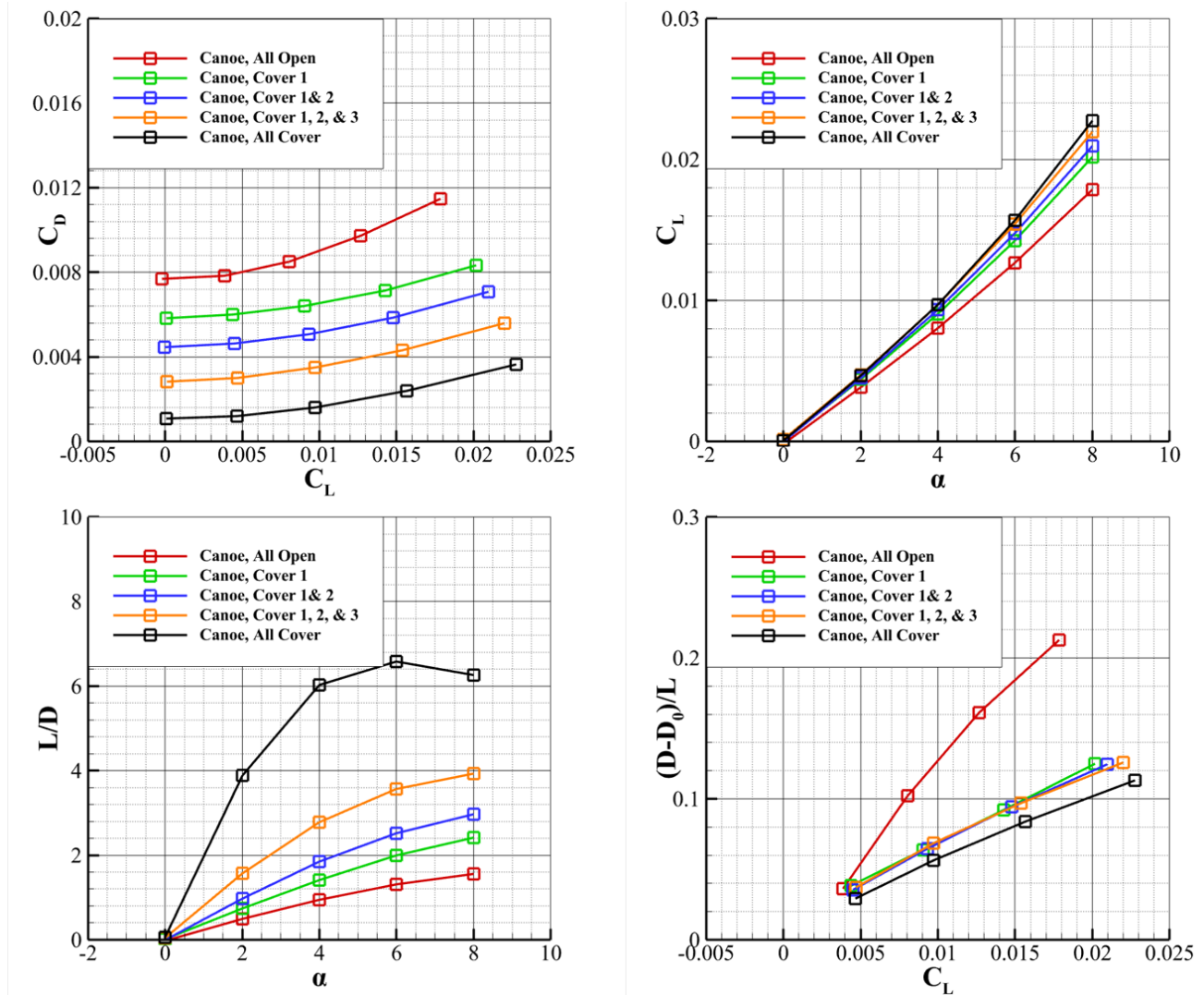


Figure 17. Aerodynamic properties of canoe case with covering of consecutive rotor openings.

Finally, the same simulation was carried out for canoe cases integrated with the wing to ensure that the drag reduction observed above was still significant on a more representative scale of geometry. The rotor-naming convention followed that presented in Figure 14 and is presented again in Figure 18 with the current configuration of interest. The result of the simulation is presented in Figure 19. Quantitatively, covering rotor number 1; numbers 1 and 2; and numbers 1, 2, and 3 would yield drag reductions of 22%, 33%, and 38%, respectively, as compared to the all-open case. These results offer quantitative insight into adding canoe doors to the current configurations, as additional elements introduce more weight into consideration; and adding canoe doors to certain rotor openings was more cost-effective. For the purpose of comparison, the simulation results of rod cases with wings attached were also presented in Figure 20. It was observed that with the addition of the first rotor door, the canoe case performs similarly to the single-rod case, therefore further solidifying the conclusion that the canoe configuration has more potential for drag reduction than the rod cases.

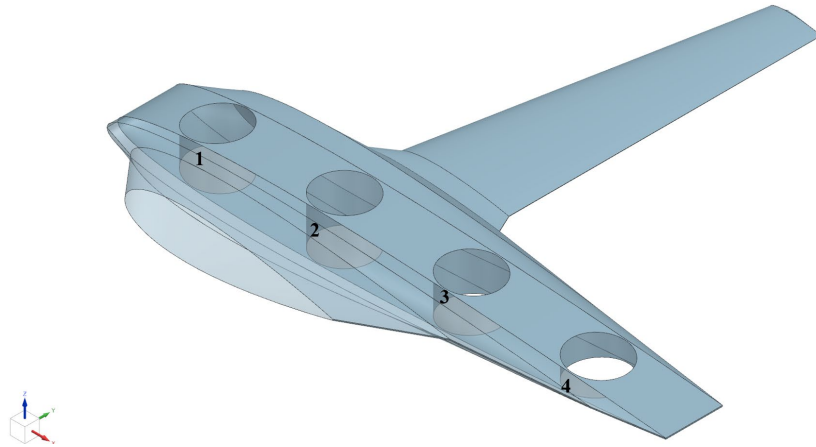


Figure 18. CAD model of canoe case integrated with wing.

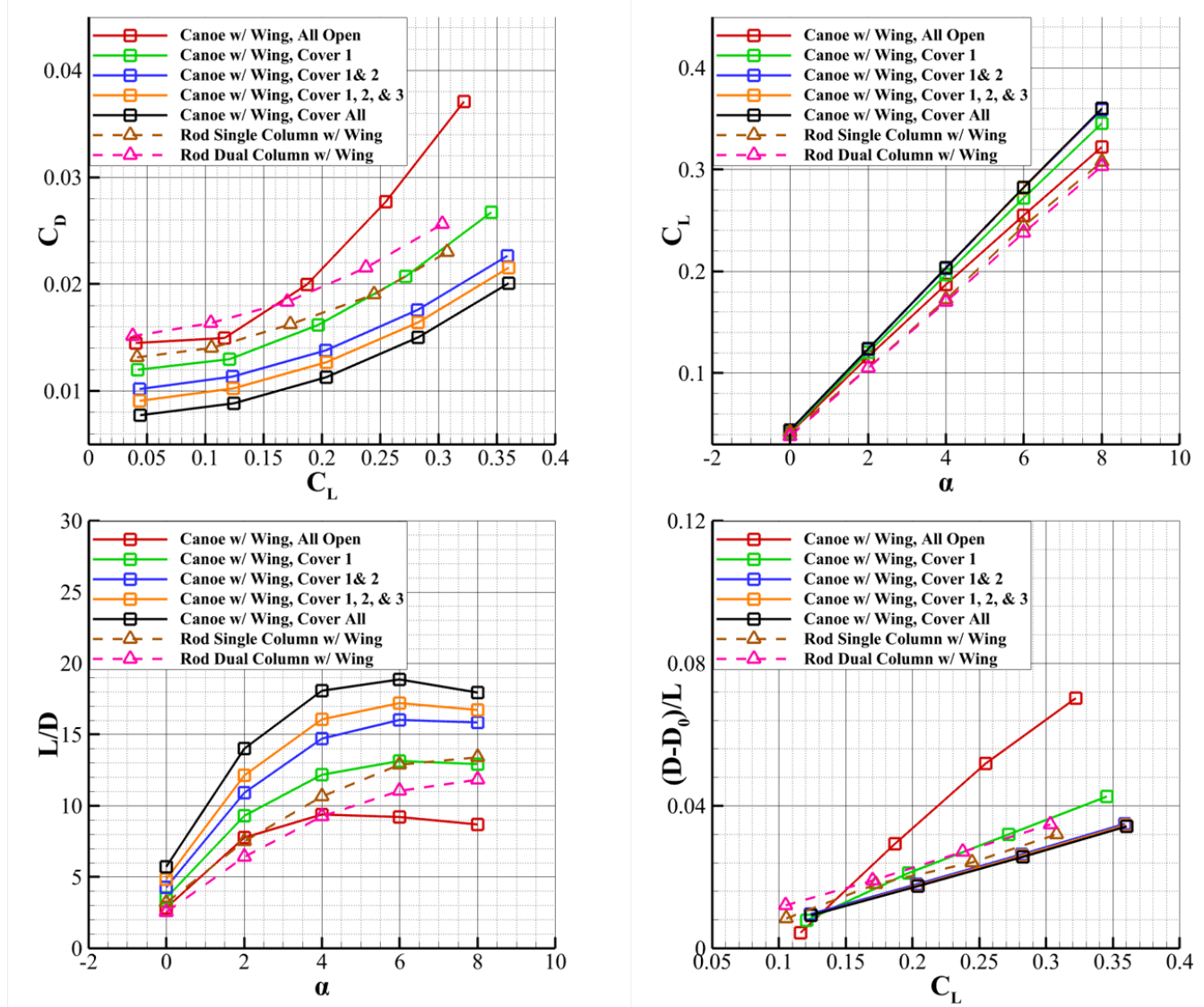


Figure 19. Aerodynamic properties of canoe cases integrated with wing.

EFFECT OF ROTOR PLACEMENT

The placement of rotors is categorized into two general approaches in the following investigation: placement in the spanwise direction and in the chordwise direction. The spanwise model consists of removing the canoe and placing rotors in a 2×2 distribution, similar to that of the rod case with dual columns instead of 1×4 distribution. The chordwise model discusses the relation between aerodynamic properties with respect to rotor distances, while holding the canoe size constant.

The two models of interest are presented in Figure 20, and the results of the simulation are presented in Figure 21. For the purpose of comparison, the simulation result of the rod case, previously shown in Figure 11, was also included. Visualization of the skin-friction coefficient magnitude across the OML is presented in Figure 22. It was observed that an opening on the lifting surface causes flow recirculation and turbulence that significantly impacts pressure distribution on surfaces behind the opening, thus it was preferred to place multiple openings along the chordwise direction to reduce their frontal projection area, i.e., lifting-surface area disturbed by openings.

The influence of the distance between rotors along the chord of the canoe was then investigated. Considering the center of mass of the entire vehicle, rotor placement was set symmetrical to the center of the canoe; and four different configurations with varying rotor distances with respect to the original canoe configuration were investigated. The distance between rotors was defined by the horizontal distance between two consecutive rotor centers and was nondimensionalized by the diameter of the rotor. For instance, Canoe O-O 2.33 \varnothing indicates that the distance between centers of two consecutive rotors was 2.33 times the diameter of the rotor. A schematic of the geometry of interest is presented in Figure 23. The results of this simulation were plotted in Figure 24. Average differences in drag, as well as geometrical differences, are presented in Table 3.

Not considering the effect of the leading edge, rotor placement does not significantly impact the aerodynamic properties of the canoe configuration. A pressure coefficient polar of the midspan of the canoe for the 2.33 diameter case and the 1.77 diameter case was plotted in Figure 25, and it was observed that pressure peaked in front of and behind each opening. This major source of drag exists independently from rotor placement, as the flow always stagnates at the opening edges facing freestream. However, if the rotors are placed too close together, for instance, the distribution in the 1.77 diameter case, the separated flow was not given enough time and space to regain kinetic energy; therefore, an increase of drag in that specific case was observed. Furthermore, it was observed that placing openings close to the leading edge causes significant flow separation by reduction in the favorable pressure gradient, causing a higher gradient of drag coefficient with respect to change in the angles of attack.

To conclude the explanation of this simulation, note that the relative distance between rotors does not have a significant impact on drag characteristics if the distance between two rotor centers is at least 175% of the diameter of the rotor. Placing the first opening away from the leading edge yields a small reduction in sensitivity of drag with respect to angles of attack, as the favorable pressure gradient of the canoe receives less disturbance.

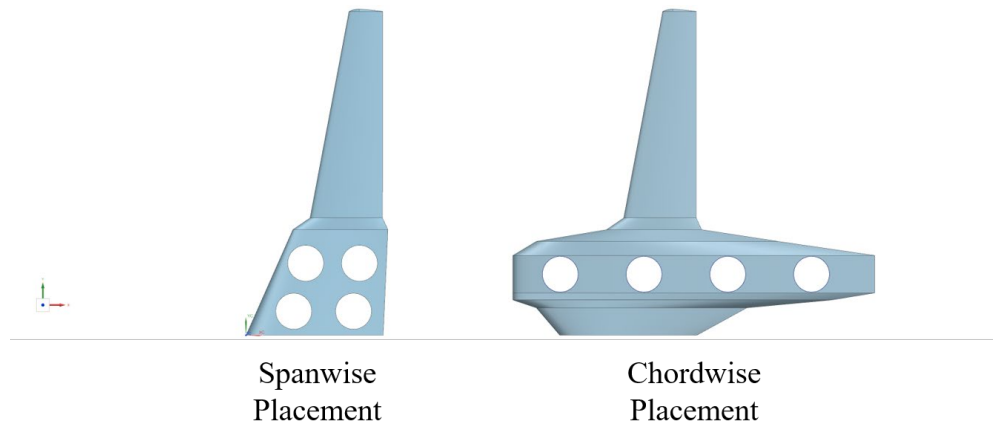


Figure 20. CAD of canoe case with various rotor-placement methods.

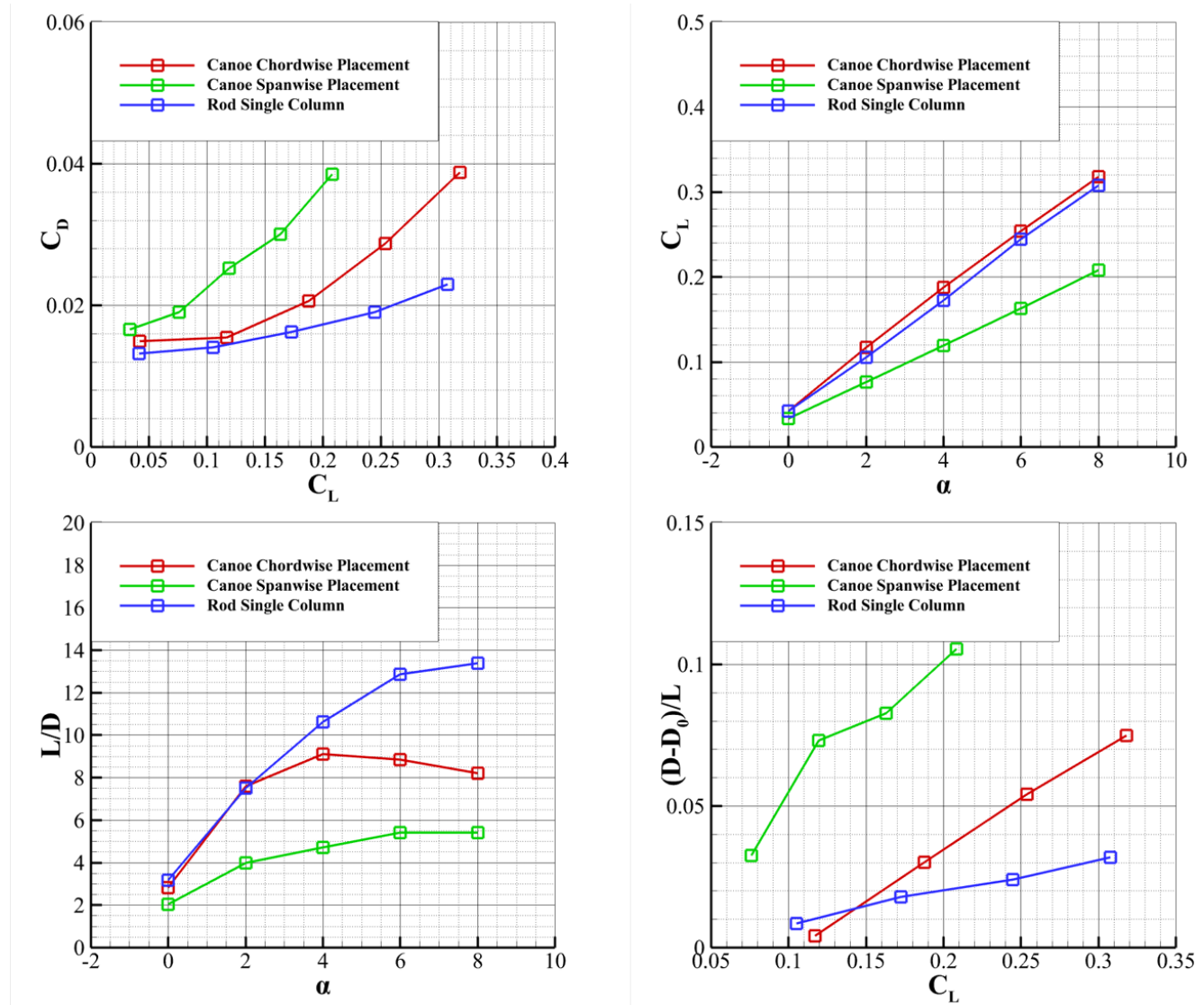


Figure 21. Aerodynamic properties of canoe case with various rotor placements.

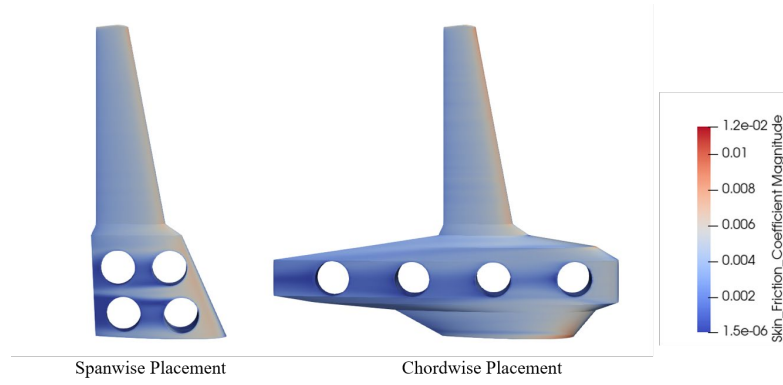


Figure 22. Visualization of CF distribution of canoe case with various rotor placements.

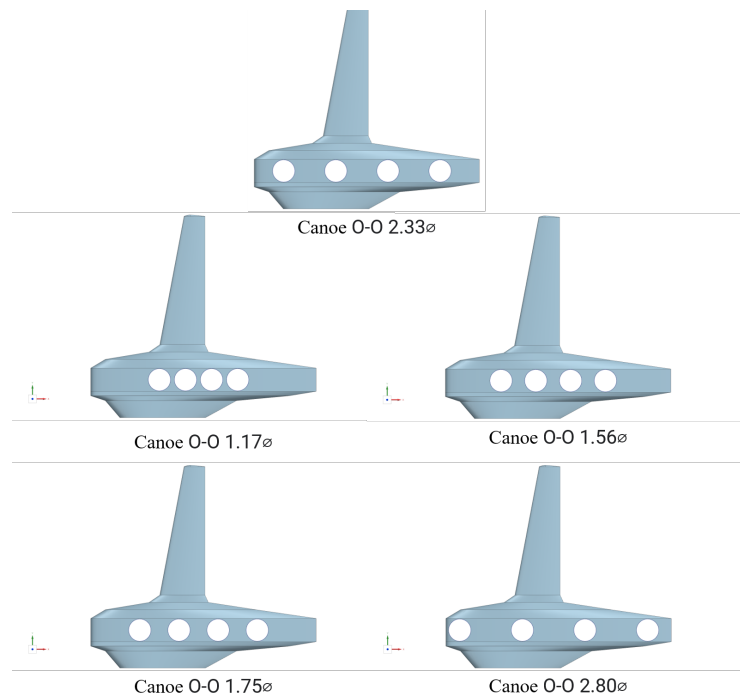


Figure 23. CAD of canoe case with various rotor chordwise distributions.

Table 3. Average Drag Difference for Various Rotor Chordwise Distributions

Distance Between Rotor Centers (ft)	Distance Nondimensionalized by Rotor Radius	Average Drag Difference (counts)	Average Percent of Drag Difference
4.59	2.33	Baseline	Baseline
2.30	1.17	3.52	1.5%
3.06	1.56	6.64	2.8%
3.44	1.75	7.44	3.1%
5.51	2.80	-14.39	-6.1%

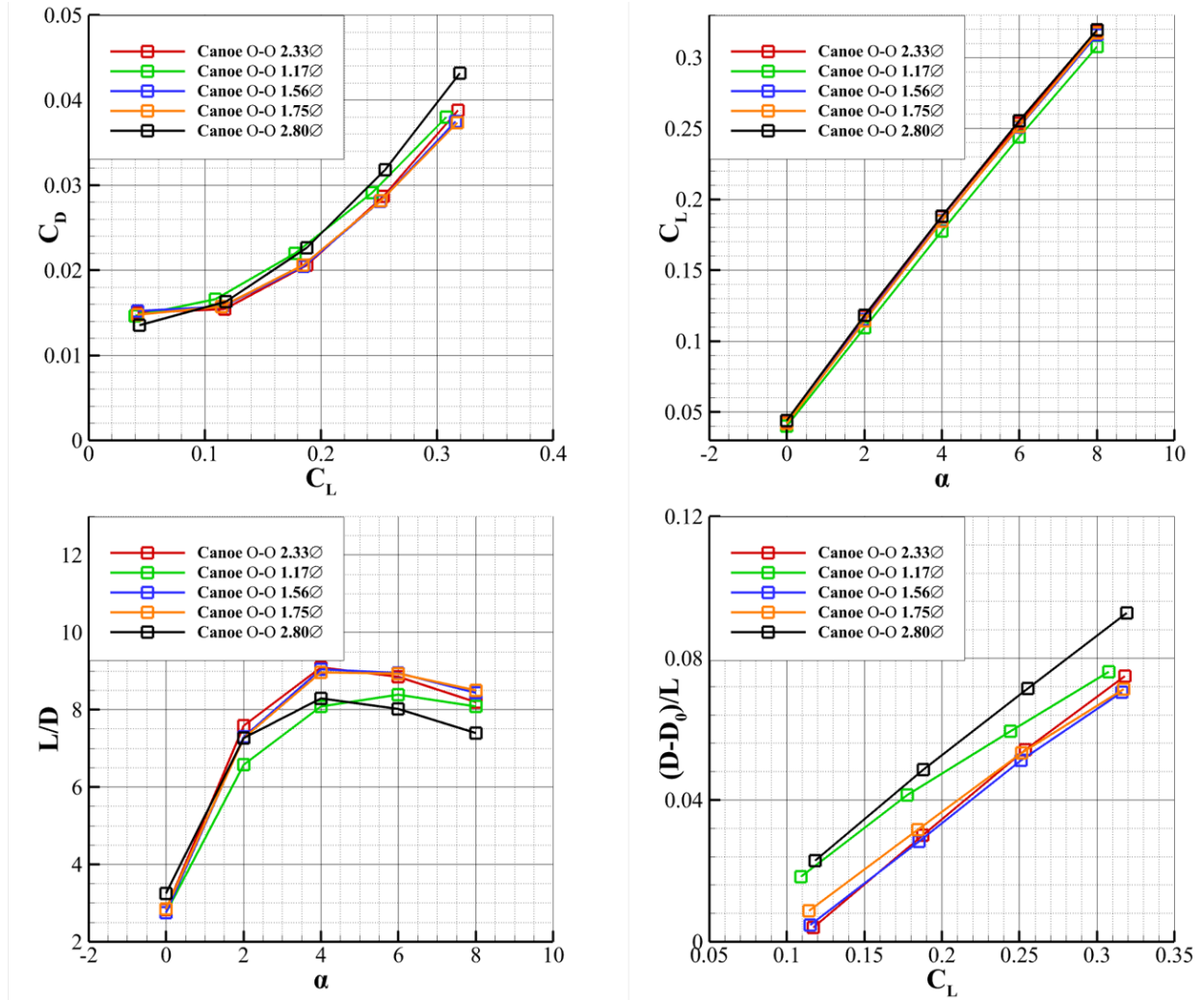


Figure 24. Aerodynamic properties of canoe case with various rotor chordwise distributions.

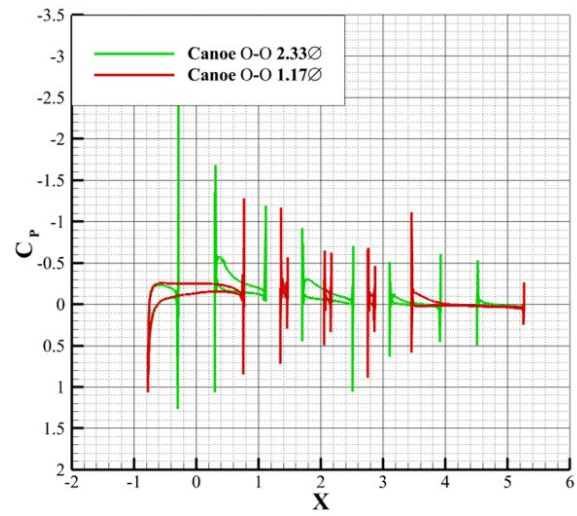


Figure 25. Pressure comparison of canoe sections with various rotor chordwise distributions.

EFFECT OF LEADING-EDGE MODIFICATIONS

A modification to the investigation described above was performed in which the absolute location of the rotors was fixed and the canoe was scaled with respect to the trailing edge in the chordwise direction, to allow a greater distance between the first opening and the leading edge. This simulation would offer insight into the absolute location of rotors with respect to the vehicle. Because pressure drag on the canoe decreases as the rotors were placed farther away from the leading edge, an extended leading edge could satisfy the aforementioned goal without clustering the rotors. Another consideration was that, if rotor doors were to be considered, a smaller curvature of the canoe outer mold line (OML) seen by the first rotor would allow easier implementation of such additional elements.

Schematics of geometries considered are presented in Figure 26, where the distance between the leading edge and the edge of the first rotor opening is nondimensionalized by rotor diameter. The result of each simulation is plotted in Figure 27. The simulation can be described as an optimization problem with conflicting objectives: It is desirable that the first opening is placed as far away as possible from the leading edge, but the extra surface area causes more skin-friction drag, which in turn diminishes the drag advantage of a configuration with an overly extended leading edge. When L/D data was plotted for a certain angle of attack, for clarification purposes chosen to be 8 degrees for all configurations investigated above, as in Figure 28, it was found that the increase follows almost a parabolic function, for which slope diminishes as the distance of interest increases.

Another related question was whether the leading-edge modification would affect the effectiveness of adding the first rotor door. Intuitively, it would seem that the sensitivity of aerodynamic performance with respect to OML changes, i.e., rotor openings, would be higher at the leading edge, thus it was likely that closing the first rotor would not be as beneficial for geometries with a longer canoe chord. To address this concern, a set of simulations with varying canoe sizes as described above and a covered first rotor was conducted. The geometries of interest are presented in Figure 29 and the results are presented in Figure 30. For the purpose of comparison, data from the respective cases with all rotors open are also presented in Figure 30. It was observed that once the first rotor was closed, drag reduction caused by increasing canoe chord became trivial; and unlike observations made in Figure 27, the case with the shorter leading edge would slightly outperform the other two cases of interest. It was also observed that reduction of drag caused by closing the first rotor decreases as the leading edge increases. The observations confirm the explanation offered at the beginning of this paragraph.

Respective drag differences in the above simulations are summarized in Table 4. If no rotor door was added, the desired distance between the first rotor and leading edge was about 2.8 times the diameter of the rotor opening. This value is prone to decrease as other driving variables such as weight, stability, and aeroelasticity are taken into consideration. Drag reduction caused by increasing the distance from the leading edge to the first rotor was trivial, as compared to that caused by covering the first rotor opening; and a longer canoe increases surface-friction drag when the rotors are covered. Therefore, adding rotor doors is a more effective choice for decreasing drag, as compared to increasing canoe chord length.

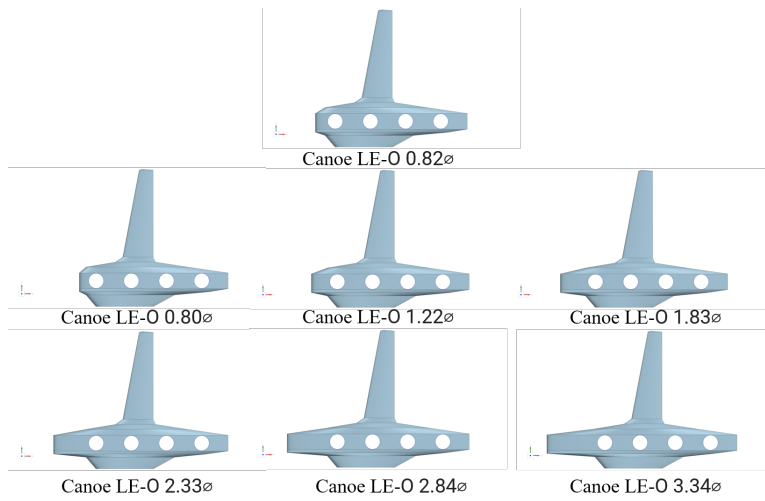


Figure 26. CAD of canoe case with various canoe chord lengths.

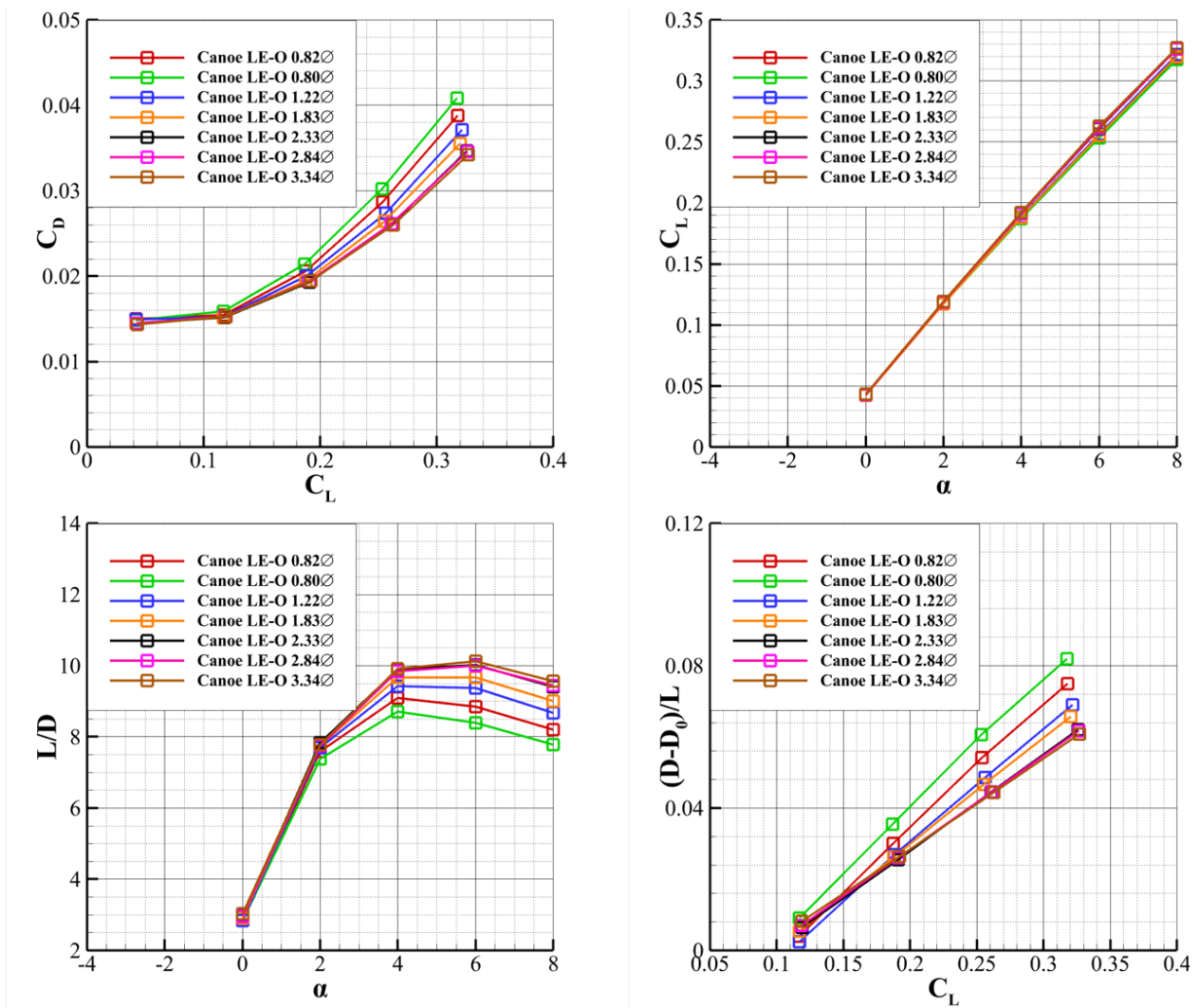


Figure 27. Aerodynamic properties of canoe case with various canoe chord lengths.

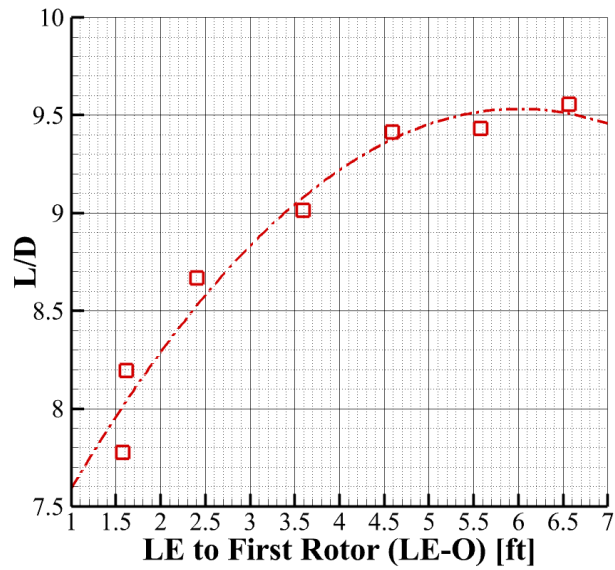


Figure 28. L/D of canoe case with various canoe chord length at an 8-degree angle of attack.

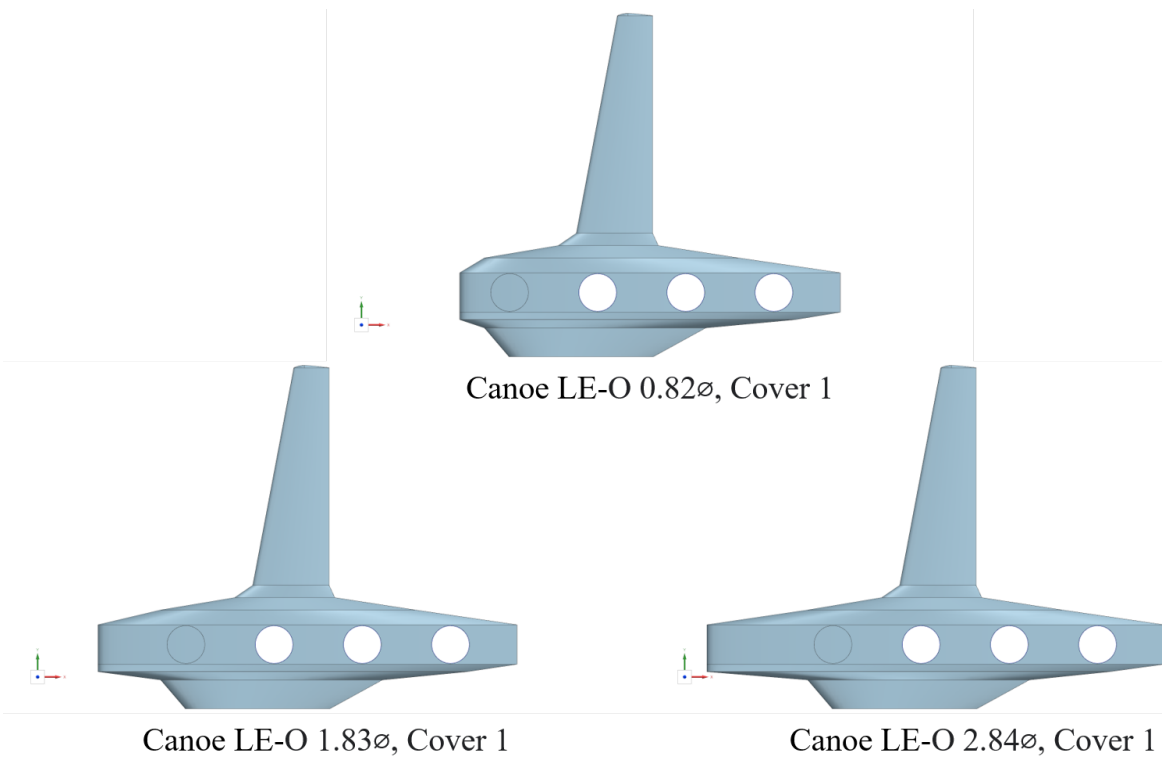


Figure 29. CAD of canoe case with various canoe chord lengths, with rotor 1 covered.

Table 4. Average Drag Difference for Various Canoe Chord Lengths

Cases	Average Drag Reduction (counts)	Average Percent of Drag Reduction
Canoe LE-O 0.82Ø	Baseline	Baseline
Canoe LE-O 0.80Ø	-9.11	-3.8%
Canoe LE-O 1.22Ø	7.89	3.3%
Canoe LE-O 1.83Ø	15.06	6.4%
Canoe LE-O 2.33Ø	17.81	7.5%
Canoe LE-O 2.84Ø	17.34	7.3%
Canoe LE-O 3.34Ø	18.69	7.9%
Canoe LE-O 0.82Ø, Cover 1	60.00	25.3%
Canoe LE-O 1.83Ø, Cover 1	56.00	23.6%
Canoe LE-O 2.84Ø, Cover 1	51.38	21.7%

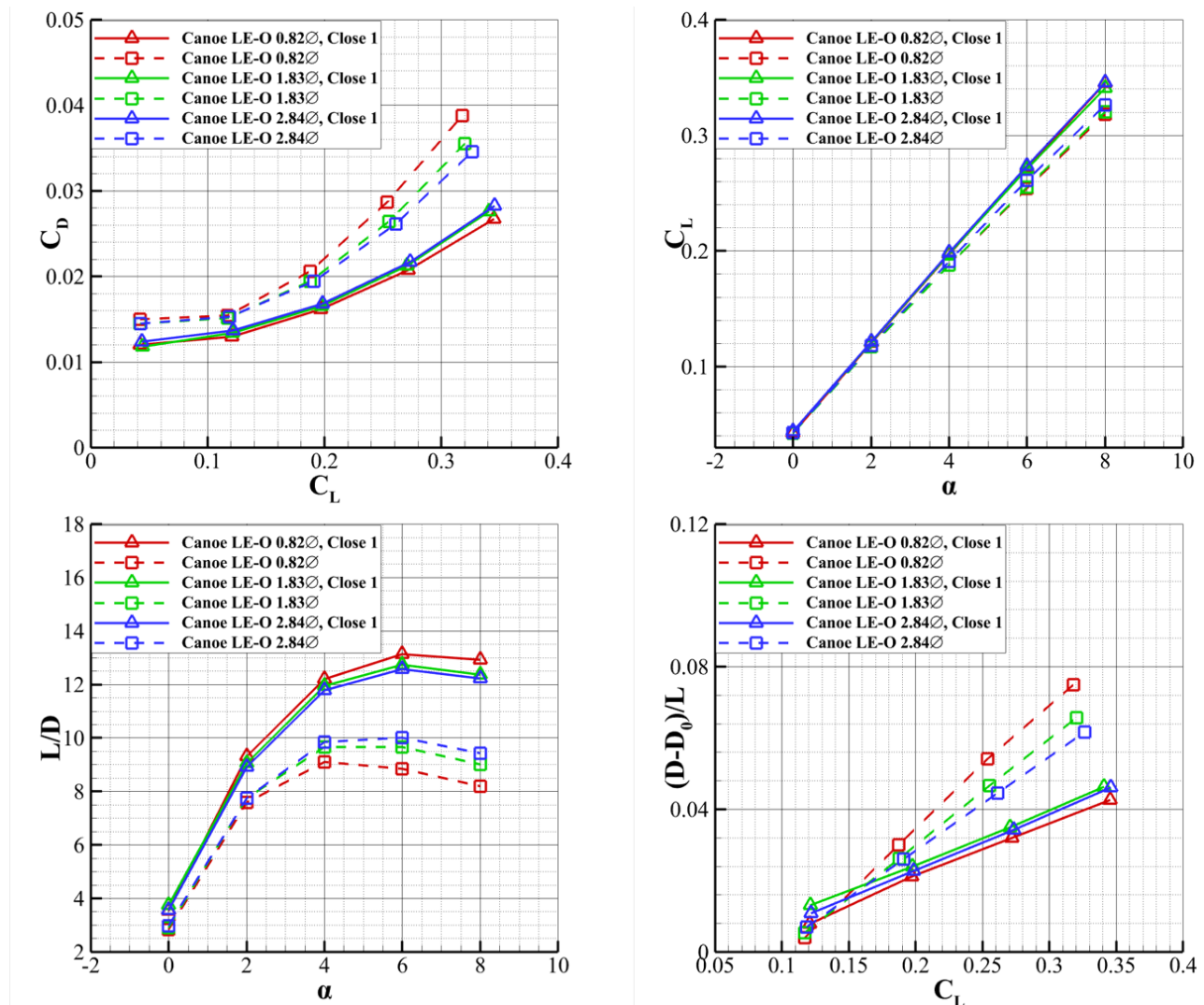


Figure 30. Aerodynamic properties of canoe case with various chord lengths, rotor 1 covered.

EFFECT OF ROUNDING ROTOR EDGES

A rounded rotor edge would facilitate better propulsive efficiency of lifting fans by increasing intake area and thus vertical mass flow rate. Furthermore, a rounded edge might allow the stagnate flow to be better attached to the surface OML, thus reducing turbulence caused by separation. A configuration with rounded rotor openings at the suction surface was made by expanding rotor diameters by half on the canoe surface. A pressure coefficient (C_p) distribution along the geometry of interest is presented in Figure 31, and C_p distribution along the midspan slice of the canoe is presented in Figure 32. It was observed that the aforementioned approach did not eliminate flow stagnation but did diffuse the turbulence observed on rotor edges. A comparison of aerodynamic coefficients was made with the canoe case with straight rotor edge, presented in Figure 33. Rounding rotor edges helped decrease the sensitivity of drag to an increase in angle of attack and attained slightly better aerodynamic performance in cases with higher angles of attack. This effect was resulted by less turbulence induced by the smooth and continuous OML, as compared to the almost vertically placed straight edges around openings. However, the rounded rotor edges also increased surface area and thus would experience more drag at low angles of attack. A trade study with driving factors including weight, aerodynamic performances, and lifting-fan efficiency would have to be conducted to determine whether rounding rotor edges is necessary.

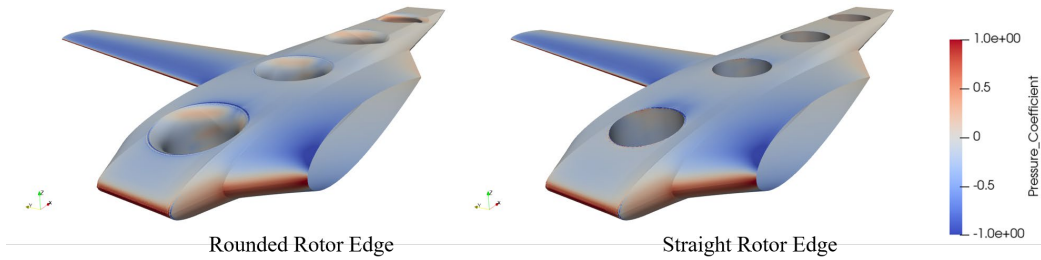


Figure 31. C_p distribution of canoe case with rounded rotor edge.

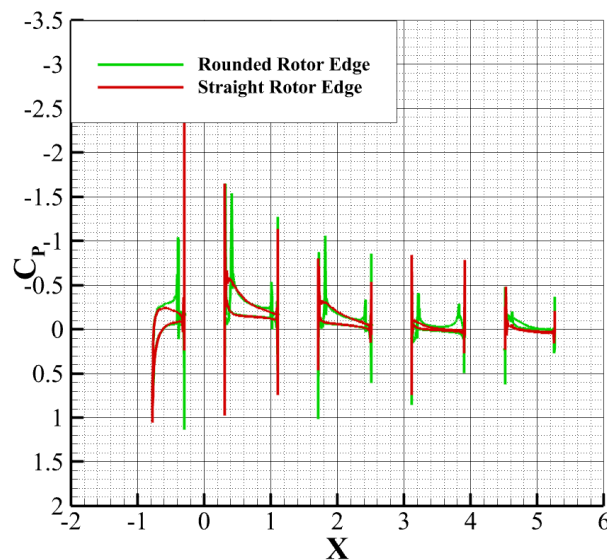


Figure 32. Pressure comparison of canoe section with rounded rotor edge.

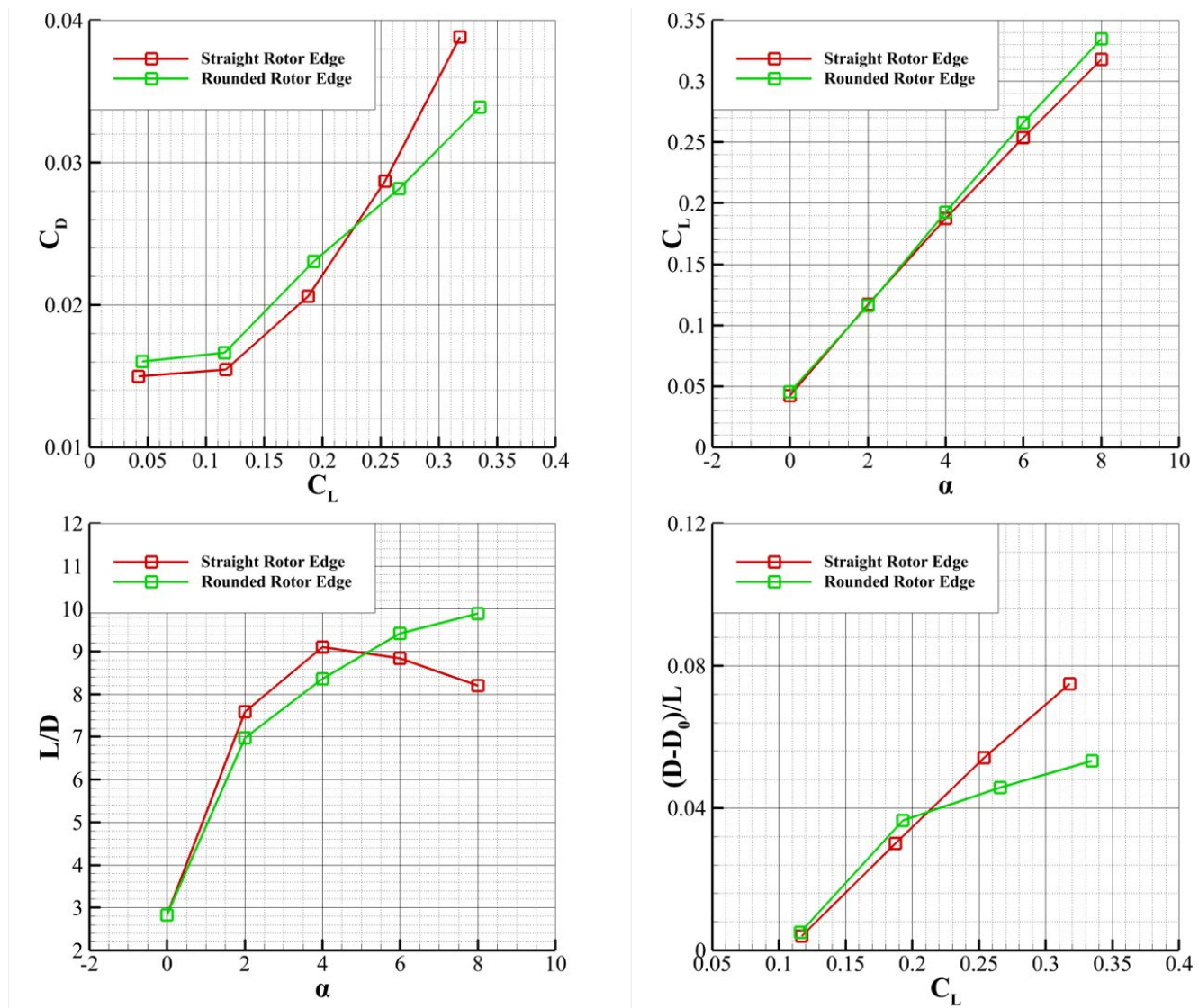


Figure 33. Aerodynamic properties of canoe case with rounded rotor edge.

EFFECT OF ROTOR DIAMETERS

The rotor diameter for the current study was set to be 1.96 ft, and a larger opening would decrease the aerodynamic performance of the current configuration. However, the major driving variable for rotor diameter was not aerodynamic efficiency but propulsive performance at vertical liftoff. Four variations of the baseline configuration with variable rotor diameter, while holding all other aspects constant, were made, as outlined in Figure 34, and simulated. The results of this simulation were plotted in Figure 35. For the purpose of comparison, results for the canoe with all rotors covered were included as an extreme case with rotor diameter equal to zero. It was observed that the relation between aerodynamic properties and diameter follows parabolic relationships. To better visualize the data and draw a correlation, a contour plot was made for L/D versus angles of attack and the diameter of rotor openings, in ft, plotted in Figure 36.

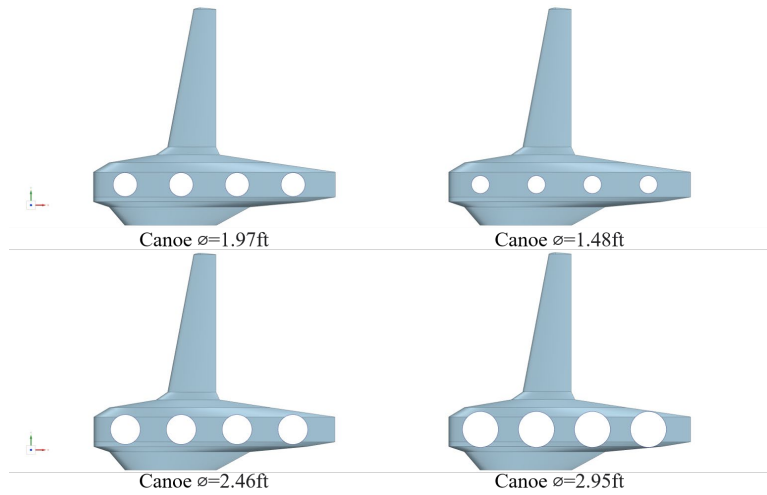


Figure 34. CAD of canoe case with various rotor diameters.

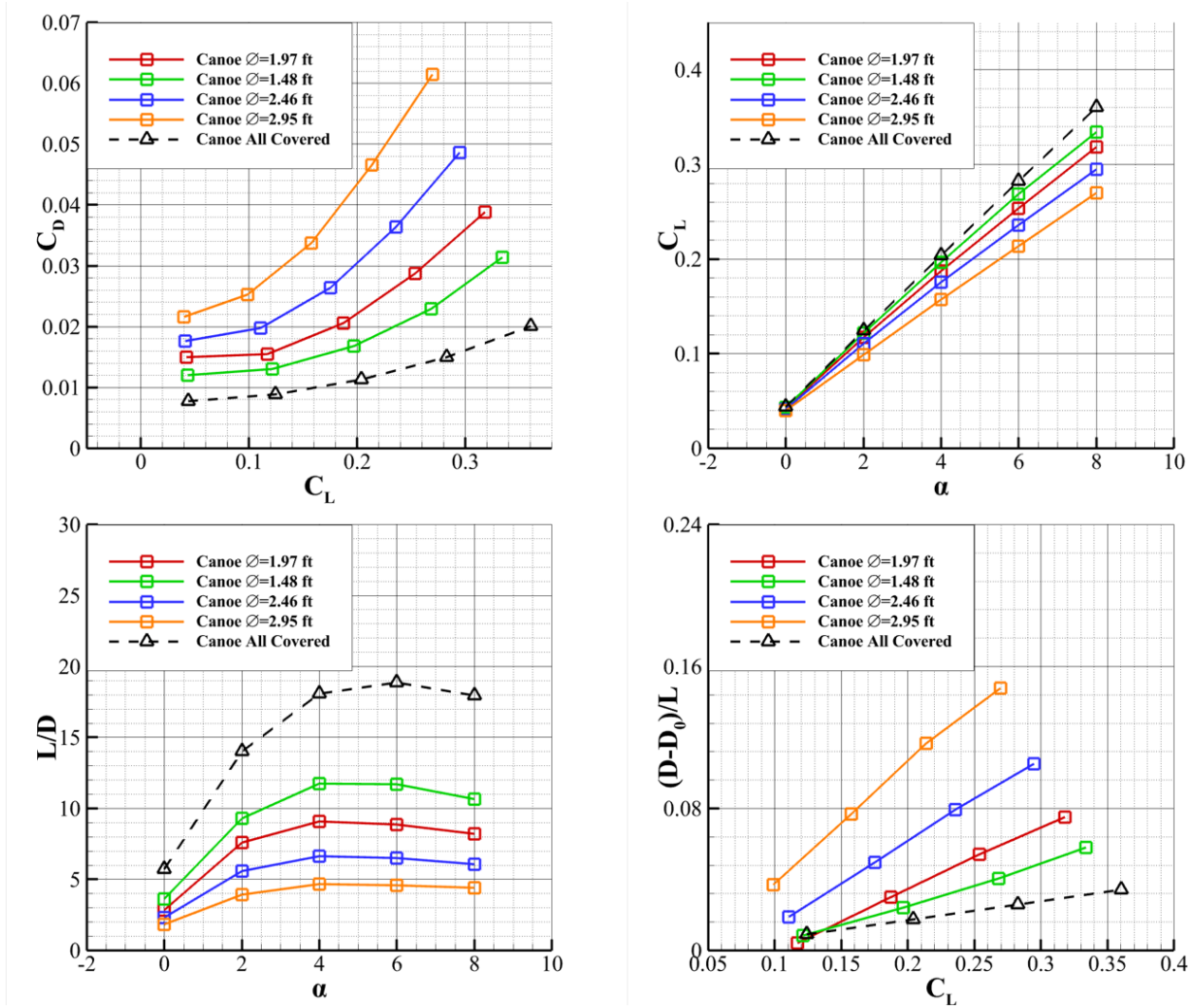


Figure 35. Aerodynamic properties of canoe case with various rotor diameters.

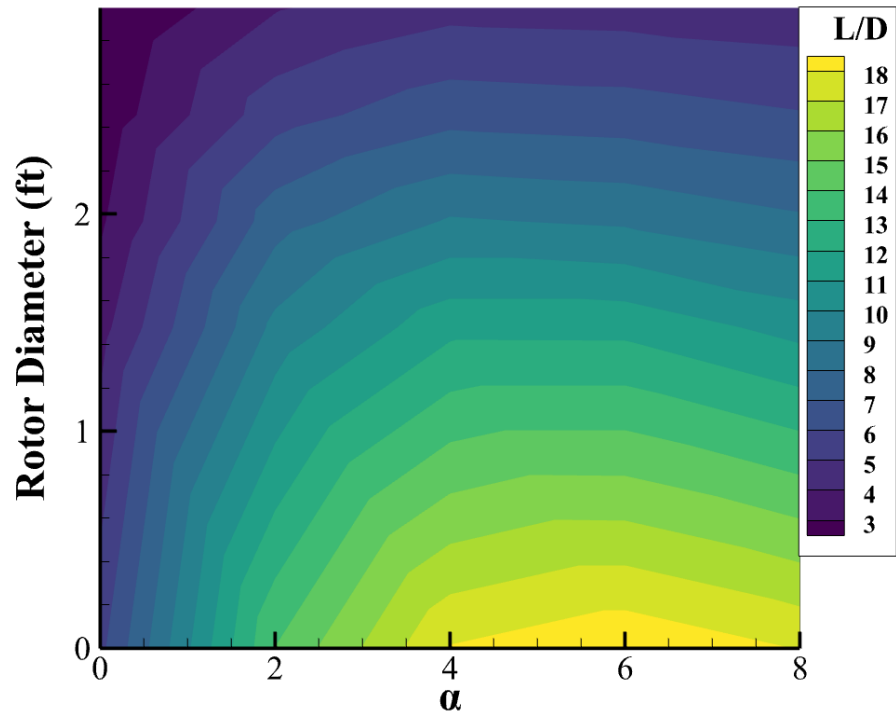


Figure 36. L/D contour of canoe case with various rotor diameters.

CHAPTER 5: FULL-CONFIGURATION SURVEY

Simulation for entire configurations, with both open and shrouded rotors, was conducted to ensure that the pros and cons of different rotor-installment methods were still significant when other components, such as fuselage and tail, were taken into consideration. The three models of interest are presented in Figure 37. Results from the simulation are presented and compared in Figure 38. Comparing these results to those presented in Figure 11, it can be observed that although fuselage and tail brought a significant amount of drag, on average 180 counts, advantages of the canoe over the rod configuration were still evident. The drag built up of fuselage and tail superpose almost linearly to aerodynamic characteristics of the wing for the canoe and the rod case, respectively.

It was also observed that the wing-fuselage junction for the rod case caused less induced drag than for the canoe case, as visualized by the C_p distribution illustrated in Figure 39. The difference in induced drag experienced was mainly due to the lack of the inversely tapered junction between the canoe and the fuselage. It would become more significant if the leading edge were extended, as compared to the baseline configuration, as discussed in Chapter 4. Possible solutions to address this concern were to extend the fuselage and remove the junction between the canoe and fuselage, by which moving the entire wing section inboard, or to decrease canoe chord length and add rotor doors to the first two openings.

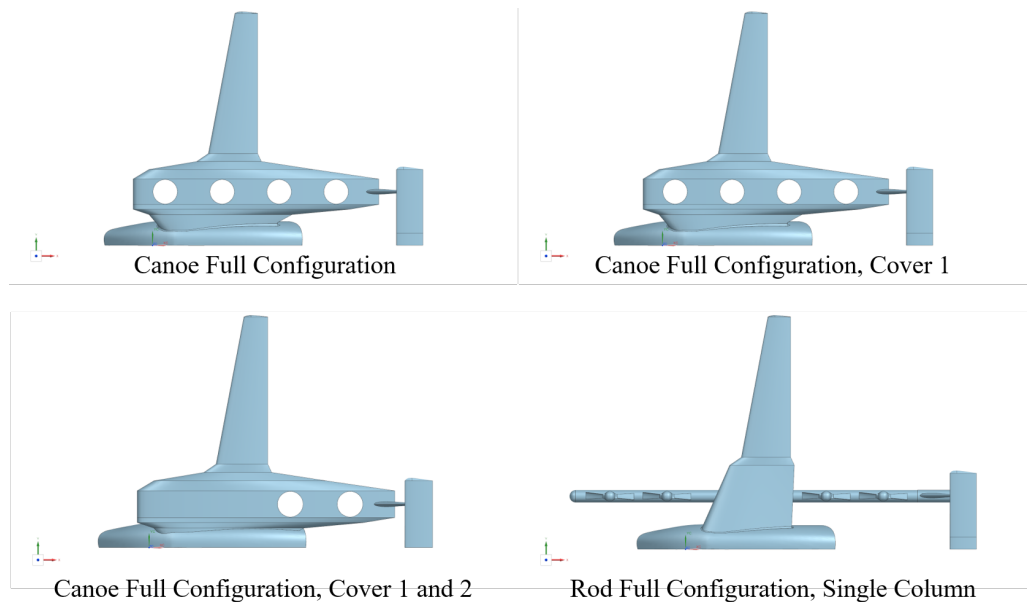


Figure 37. CAD of canoe and rod cases with fuselage and tail.

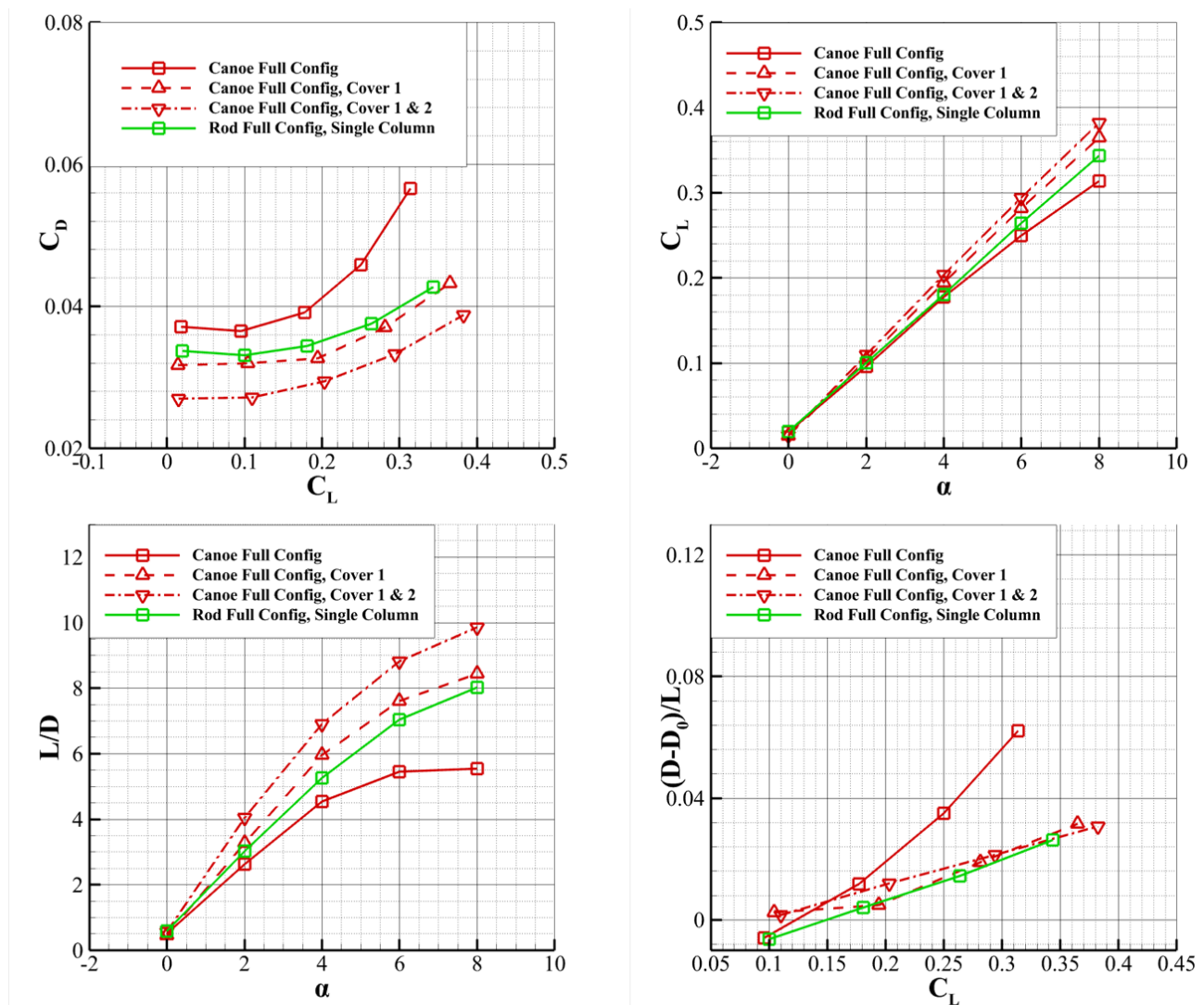


Figure 38. Aerodynamic properties of full configurations.

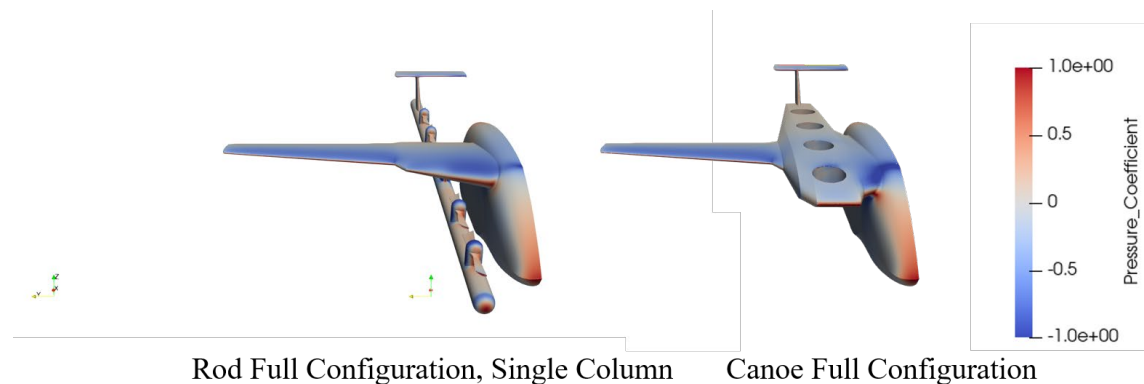


Figure 39. C_p distribution of full configurations.

CHAPTER 6: CONCLUSION AND FUTURE WORK

This study investigated aerodynamic properties of different eVTOL designs, as well as potential modifications of the canoe configuration. Modifications and driving factors considered in this study included rotor doors, rearranging rotor placement, canoe sizing, and rotor diameters; and results were arrived at individually, as follows. A summary of all configurations investigated above was summarized in Table 5. The angle of attack of 2 degrees was chosen to be a representative flight condition in Table 5, and the order of trade elements followed that presented in this report. Trade elements that have significant impact on drag were highlighted using asterisks.

Varying canoe thickness does not significantly change drag characteristics: As decreasing canoe thickness by 25%, with last two rotors open, increased drag coefficient by 5 counts, and decreasing canoe thickness by 25%, with all rotors sealed, decreased drag coefficient by 10 counts. This variation was small, as compared to the advantage brought by changing leading-edge length or adding canoe doors.

Rotor doors significantly improve the drag characteristics of the canoe case. Both upper and lower surfaces of a rotor opening need to be closed to achieve optimal results; and closing the first three rotor openings can achieve on average 38%, or 100 counts, of drag-coefficient reduction. Among all rotor doors, closing the ones closest to the leading edge has a better effect in reducing drag than closing those near the trailing edge; and covering the first rotor causes drag coefficients similar to those of the rod single-column case.

Rotors should be placed vertically in the chordwise direction to reduce their frontal projection area. The separated flow was observed after each rotor opening, thus placing rotors in the spanwise direction impacts the effectiveness of the wing. Placing rotors closer together does not significantly influence the aerodynamic performance of the geometry; but placing the first opening closer to the leading-edge results in early separation, caused by decreased favorable pressure gradient regime. If no rotor doors are added, the first opening should be placed 2.8 times the rotor diameter away from the leading edge for drag reduction. If rotor doors are added, drag reduction caused by leading-edge modification was small; and the distance between the leading edge and the first rotor can be left as small as possible.

Significant stagnation was observed at the opening edges facing directly toward or against the freestream. Flow stagnation in the aforementioned area was identified as a major source of pressure drag in the current configuration. Rounding rotor openings did not impact drag experienced but could be added to facilitate vertical mass flow rate when running lifting fans.

The effect of rotor diameter on drag characteristics of the canoe configuration was shown to display a parabolic relationship. Openings of larger diameter increase drag experienced by the canoe, but it is important to note that the main driver of rotor diameter was propulsive efficiency at liftoff rather than aerodynamic efficiency at cruise.

Table 5. Summary of Trade Elements and Respective Drag Differences

Trade Element	Baseline	New	Baseline CD at AoA 2 (counts)	New CD at AoA 2 (counts)
Rod/Canoe with Wing*	Canoe	Rod Single Column	154.47	140.29
Canoe Thickness	1.2 ft	0.9 ft	113.25	113.42
Canoe Door*	All Open	Cover 1	154.47	129.48
Canoe Door*	All Open	All Covered	154.47	88.62
Canoe Rotor*	Single Column	Dual Column	154.47	190.38
Canoe Rotor Spacing	O-O 2.33Ø	O-O 1.56Ø	154.47	157.51
Leading Edge*	LE-O 1.22Ø	LE-O 2.84Ø	154.47	118.47
Leading Edge	LE-O 1.22Ø	LE-O 0.80Ø	154.47	158.61
Leading Edge	LE-O 1.22Ø, 1 Covered	LE-O 2.84Ø, 1 Covered	129.48	136.61
Round Rotor Edge*	Straight	Rounded	154.47	166.24
Rotor Diameter	Ø=1.97ft	Ø =1.48ft	154.47	130.47
Rotor Diameter*	Ø=1.97ft	Ø=2.95ft	154.47	252.51
Full Configuration*	Canoe, All Open	Rod Single Column	365.00	330.69
Full Configuration*	Canoe, All Open	Canoe Cover 1	365.00	319.32

*Element that results in significant aerodynamic property changes.

When the configurations were simulated with other components, such as tail and fuselage, the improvements and advantages mentioned above were still significant. Flow separation was observed at the inboard edge of the canoe, and the wing–fuselage junction of the canoe case received more drag than that of the rod case.

Future studies should be based on a new configuration integrating all the suggestions mentioned above. A first representation of the next design iteration is presented in Figure 40. The new configuration, as compared to the ones discussed in this report, improves upon the canoe case with a shorter canoe, the first two rotors covered by rotor doors, more compact rotor spacing, rounded rotor edges, and better wing–fuselage junction. Future studies should also discuss different shapes of fuselage and their aerodynamic properties. For the current study, the fuselage was only initially discussed, and a large separation was observed behind the vertical end of the fuselage. Stability of this vehicle should also be taken into consideration in the future, as the suggested shortening of the canoe may interfere with control efficiency of the tail. Finally, an MDO problem could be performed on the wing–canoe junction for better performance. The problem would consider weight, aeroelasticity, and aerodynamics as objectives and optimize the wing OML to better fit the mission profile.

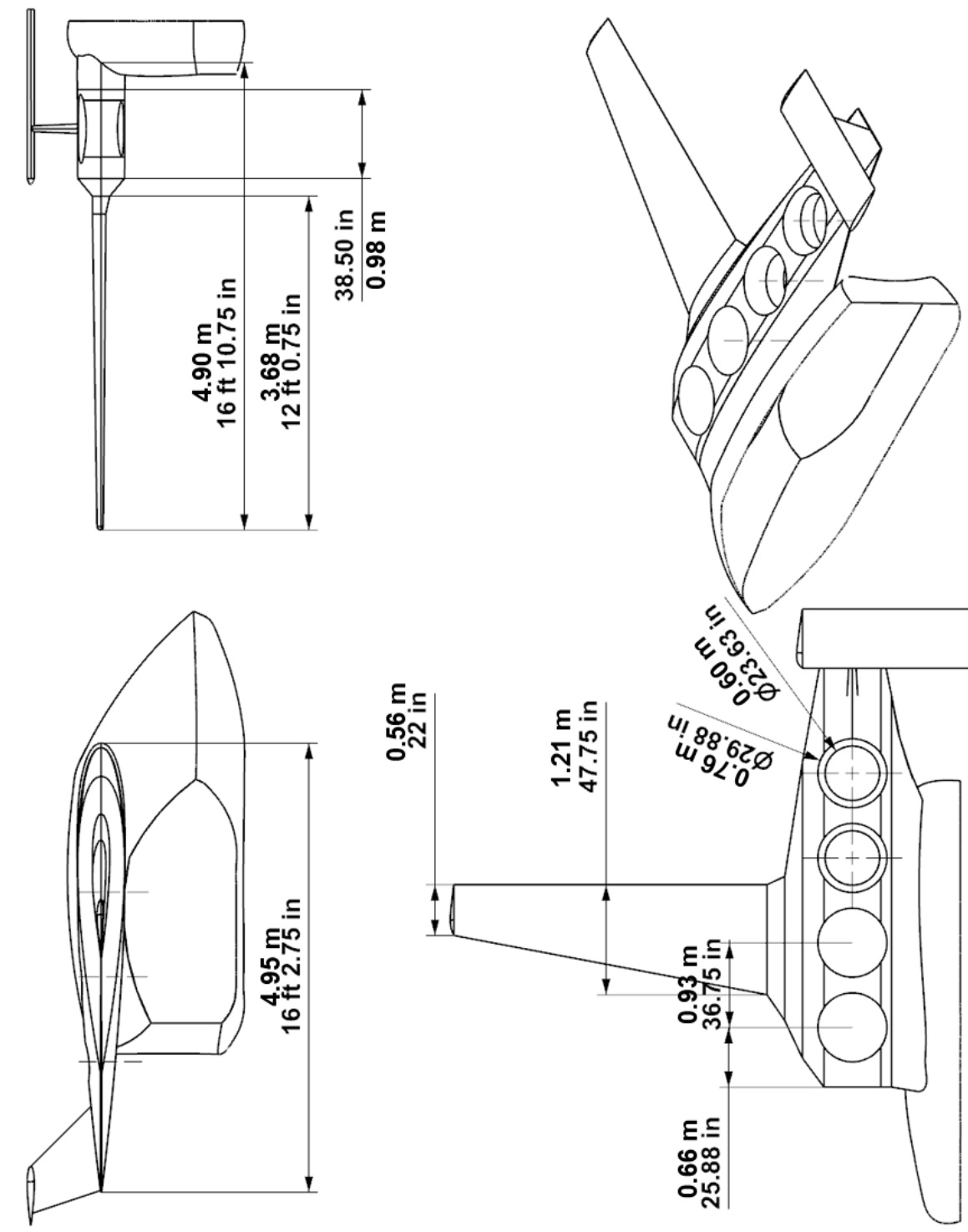


Figure 40. CAD of possible new configuration.

REFERENCES

- [1] Ng, W., Patil, M., and Datta, A., "Hydrogen Fuel Cell and Battery Hybrid Architecture for Range Extension of Electric VTOL (eVTOL) Aircraft," *Journal of the American Helicopter Society*, 66(1): 1–13, 2021. <https://doi.org/10.4050/jahs.66.012009>. [retrieved 22 March 2022].
- [2] Moore, M., "NASA Puffin Electric Tailsitter VTOL Concept," 10th AIAA Aviation Technology, Integration, and Operations (ATIO) Conference, 2010, pp. 13–15, American Institute of Aeronautics and Astronautics, doi:10.2514/6.2010-9345. [retrieved 22 March 2022].
- [3] "AHS International Leads Transformative Vertical Flight Initiative." *News on electric vertical takeoff & landing (eVTOL) aircraft*, <https://evtol.news/news/ahs-international-leads-transformative-vertical-flight-initiative>. [retrieved 22 March 2022].
- [4] "Pioneering the Urban Air Taxi Revolution," Volocopter, 6 June 2019, <https://www.volocopter.com/wp-content/uploads/Volocopter-WhitePaper-1-01.pdf> [retrieved 22 March 2022].
- [5] Home Page, Tier 1 Engineering, <https://www.tier1engineering.com/> [retrieved 22 March 2022].
- [6] "Urban Air Mobility," Volocopter, <https://www.volocopter.com/urban-air-mobility/> [retrieved 22 March 2022].
- [7] "Pipistrel unveils 801 Evtol at Uber's Elevate Summit," Pipistrel Aircraft, <https://www.pipistrel-aircraft.com/pipistrel-unveils-801-evtol-at-ubers-elevate-summit-archive/> [retrieved 22 March 2022].
- [8] Joby Aviation, Joby, <https://www.jobyaviation.com/> [retrieved 22 March 2022].
- [9] "Lilium jet—the first electric VTOL (EVTOL) jet," Lilium, <https://lilium.com/jet> [retrieved 22 March 2022].
- [10] "Evtol classifications, News on electric vertical takeoff & landing (eVTOL) aircraft," <https://evtol.news/classifications/> [retrieved 22 March 2022].
- [11] Hascaryo, R. W., and Merret, J.M., "Configuration-Independent Initial Sizing Method for UAM/eVTOL Vehicles," American Institute of Aeronautics and Astronautics Aviation 2020 Forum, <https://doi.org/10.2514/6.2020-2630>.
- [12] Economou, T. D., Palacios, F., Copeland, S. R., Lukaczyk, T. W., and Alonso, J. J., "SU2: An Open-Source Suite for Multiphysics Simulation and Design," *American Institute of Aeronautics and Astronautics Journal*, 54(3): 828–46, 2016. <https://doi.org/10.2514/1.J053813>.
- [13] "Mesh generation software for CFD: Pointwise, Inc.," <http://www.pointwise.com/> [retrieved 22 March 2022].